Bull Volcanol (2017) 79: 23
DOI 10.1007/s00445-017-1103-2

RESEARCH ARTICLE

Diatreme evolution during the phreatomagmatic eruption of the Songaksan tuff ring, Jeju Island, Korea

S.Y. Go[1] · G.B. Kim[1] · J.O. Jeong[2] · Y.K. Sohn[1]

Received: 14 September 2016 / Accepted: 29 January 2017 / Published online: 16 February 2017

Abstract The Songaksan tuff ring, Jeju Island, Korea, which erupted ca. 3.7 ka BP in a coastal setting, provides an unusual opportunity to study the processes of phreatomagmatic eruption and the formation of a diatreme because of the exceptionally well-preserved ejecta beds and well-known subsurface geology. The tuff sequence can be divided into four units (A to D), which have distinctly different accidental componentry (quartz-rich vs. quartz-poor), grain surface features (abraded and ash-coated vs. unabraded and uncoated), and chemical compositions of juvenile particles. The basal tephra bed of unit A, which probably erupted after the removal of the relatively hard shallow-level (<120 m deep) substrate by initial cratering, comprises only unabraded and uncoated grains and contains abundant relatively deep-derived (>120 m deep) accidental grains, suggesting that the early erupted tephra had not yet experienced recycling and pre-eruption mixing in the diatreme. On the other hand, the overlying tephra beds of units A, B, and D contain an abundance of abraded and ash-coated juvenile/accidental grains, suggesting that the tephra comprised significant proportions of "recycled" or "premixed" materials from previous eruptions or subsurface explosions, which participated in the explosion-driven mixing in the diatreme before eventual ejection from the diatreme. Unit C is unusual in that it comprises extremely rare accidental grains and ash-coated juvenile/accidental grains. We interpret that the supply of solid materials, either accidental or juvenile, to the diatreme was greatly reduced because of temporary stabilization of the diatreme and the reduction in magma flux to the diatreme. The diatreme is therefore envisaged to have been filled with a water-saturated slurry, in which particle abrasion and adhesion were inhibited. We also infer that the diatreme fill was temporarily removed by a powerful explosion before eruption of unit C on the basis of the near absence of the tephra grains from earlier eruptions throughout the tephra beds of unit C. The ratio of tachylite to sideromelane grains generally increases up-section of the tuff sequence with two abrupt drops across the tuff unit boundaries. These variations are coincident with the changes in the chemical composition of juvenile particles, suggesting an overall decrease in magma flux punctuated by brief increases in magma flux associated with the arrival of new magma batches. The textural and compositional variations of the Songaksan tuff ring suggest that there can be significant variability in diatreme processes even during a purely phreatomagmatic eruption of a tuff ring, including removal and renewal of the diatreme fill, and that there is still much room for further investigation of the diatreme processes from the ejecta beds in order to make the current diatreme model more robust.

Keywords Tuff ring · Diatreme · Phreatomagmatism · Magma-water interaction · Tephra componentry · Jeju Island

Editorial responsibility: P-S Ross

✉ Y.K. Sohn
yksohn@gnu.ac.kr

[1] Department of Geology and Research Institute of Natural Science, Gyeongsang National University, Jinju 52828, Republic of Korea

[2] Center for Research Facilities, Gyeongsang National University, Jinju 52828, Republic of Korea

Introduction

Tuff rings and maars are monogenetic volcanoes that have a low-profile apron of tephra surrounding a wide crater (Vespermann and Schmincke 2000). The classic distinction between maars and tuff rings is that when the crater is cut into the pre-eruption surface, the volcano is called a maar; otherwise, it is a tuff ring (Lorenz 1973). However, we do not consider that maars and tuff rings are truly distinct volcano types. Many tuff

rings with crater floors seemingly above pre-eruption surfaces actually have craters that were cut into pre-eruption surfaces but were buried later. We are skeptical whether there is a "true" tuff ring, of which the crater has never been cut below the pre-eruption surface. Both tuff rings and maars are thought to form largely from phreatomagmatic explosions in the subsurface (Lorenz 1986; Sohn 1996; White 1996; White and Houghton 2000) and are underlain by a diatreme, which is a conical to cylindrical structure filled with a mixture of juvenile and country rock materials, plus intrusions (White and Ross 2011). The diatremes under maars extend downward hundreds of meters to more than a kilometer below the pre-eruption surface and merge into a feeder dike (White and Ross 2011). Maars are also called "maar-diatreme volcanoes" because a diatreme is an integral part of these volcanoes and has a volume comparable to that of the volcanic edifice on the surface.

Diatremes have been increasingly studied in recent years because of their significance in understanding a suite of phreatomagmatic processes, i.e., from the inception of magma-water interaction in the subsurface to final emplacement of ejecta on the surface around the vent as an ejecta/tephra ring. Diatremes are, however, observable only where a volcanic field has been eroded well below the pre-eruption surface (e.g., White 1991; Ross and White 2006; Geshi et al. 2011; Son et al. 2012; Lefebvre et al. 2013; Delpit et al. 2014). Many studies have therefore relied upon the analysis of ejecta rings (especially not only those of maars but also of tuff rings) in order to understand the subsurface diatreme processes because much information can be drawn from the analyses of both juvenile and accidental materials within the ejecta rings. The processes and features that can be studied using ejecta rings include the lithology and rigidity of the substrate, the type of aquifer, the depth and modes of magma-water interactions, and the mechanisms and extent of country rock excavation and entrainment (Rosseel et al. 2006; Auer et al. 2007; Sottili et al. 2009; Ross et al. 2011; Valentine 2012). However, there are unavoidable limitations and uncertainties in interpreting these processes because the ejecta rings only record indirectly part of the subsurface diatreme processes (Valentine and White 2012; Lefebvre et al. 2013). These studies show that maar-diatreme volcanoes commonly experience complex eruption histories, including both phreatomagmatic and magmatic (usually Strombolian) activities, in some cases with repeated changes in eruption style during a single eruption (Houghton and Schmincke 1986; Houghton and Nairn 1991; Carrasco-Núñez et al. 2007; Sottili et al. 2009; Gernon et al. 2013). Diatremes are therefore inferred to have the characteristics that reflect these complex eruption histories in addition to a suite of processes that are inherent in the diatremes, such as intrusion and mingling of magma, explosive magma-water interaction, explosion-driven mixing and jetting of debris, explosive excavation of country rocks, and gravity-induced collapse of diatreme walls and overlying tephra beds (White and Ross 2011; Valentine and White 2012).

Songaksan is the youngest volcanic center on Jeju Island, Korea, produced by a 3.7 ka BP eruption in a coastal setting (Sohn et al. 2002) (Fig. 1). Although the volcano experienced a change in eruption style from phreatomagmatic to magmatic, resulting in a tuff[1] ring with a nested scoria cone and a ponded trachybasalt lava inside the crater, the entire sequence of the tuff ring is dominated by well-bedded tuffs with diverse bedforms, which indicate deposition from moist pyroclastic surges and associated fallout, without a single intercalation of tephra produced by magmatic eruptions (Chough and Sohn 1990). In addition, the subsurface geology is very well known because thousands of wells have been drilled to exploit groundwater for several decades in Jeju Island. The Songaksan tuff ring[2] thus provides an opportunity to investigate the diatreme-forming processes during a relatively simple phreatomagmatic eruption of an ejecta ring without the complicating factors of changing eruption styles and the ambiguity of subsurface hydrogeological conditions. In this paper, we investigate the processes of diatreme formation beneath Songaksan based on the componentry of ash-sized tephra from the medial-to-distal tuff ring. We show that there can be significant variability in diatreme processes even during a purely phreatomagmatic eruption.

Geological setting

Jeju Island is an intraplate basaltic volcano built on the ca. 100-m-deep Yellow Sea continental shelf off the southern coast of the Korean Peninsula (Brenna et al. 2012; Koh et al. 2013; Brenna et al. 2015) (Fig. 1a). The island was produced by widespread and prolonged hydrovolcanic activity on the continental shelf between ca. 1.8 and 0.5 Ma, and later, lava effusion after the hydrovolcanic field emerged above the fluctuating Quaternary sea level (Sohn and Park 2004; Sohn et al. 2008). The former activity produced a subsurface hydrovolcanic succession named the Seoguipo Formation, whereas the latter produced the lava shield dotted with hundreds of volcanic cones (mostly scoria cones) (Fig. 1b). Several tuff rings and tuff cones were produced on top of the lava shield in the Late Pleistocene and Holocene (Sohn et al. 2002; Cheong et al. 2007).

[1] We use terms such as "tuff ring," "tuff," and "lapilli tuff" in this paper despite the nearly unconsolidated state of the phreatomagmatic deposits at Songaksan, for convenience and for historical continuity.

[2] Using the classic distinction between maars and tuff rings based on the crater position relative to the pre-eruptive surface, Songaksan is probably a maar. We cannot see the crater floor of the tephra ring at Songaksan because it is filled by later scoria cones and ponded lava. However, the crater must have been cut into the pre-eruption surface near sea level before it was filled by these later volcanic deposits, as evidenced by the sea cliff exposures [see Fig. 3a of Sohn et al. (2002)], which show the inner crater wall of the ejecta ring dipping ~45° and apparently extending below the pre-eruption surface. The abundance of accidental materials at Songaksan also argues for a maar. However, we still use the term Songaksan tuff ring here, for historical continuity and because we do not consider maars and tuff rings to be distinct volcano types.

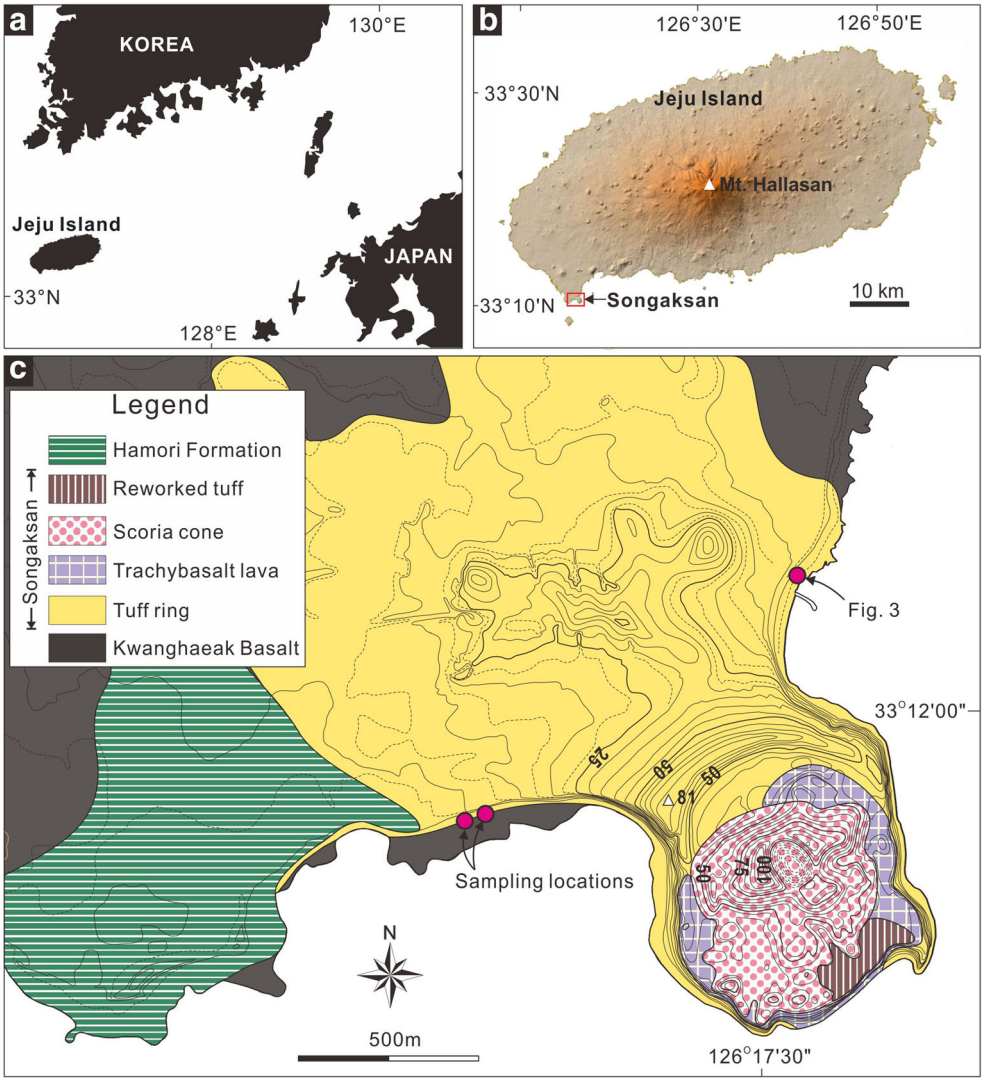

Fig. 1 **a** Location map of Jeju Island. **b** Digital elevation model of Jeju Island consisting of a broad and gently sloping lava shield and a 1950-m-high central peak (Mt. Hallasan) dotted by numerous volcanic cones. **c** Geologic and topographic map of Songaksan, which consists of a tuff ring with a nested scoria cone and a ponded trachybasalt lava inside the crater. The Kwanghaeak Basalt beneath Songaksan, Late Pleistocene in age, forms a gently undulating coastal plain in southwestern Jeju Island. The Hamori Formation is the product of post-eruptive erosion and reworking of the Songaksan tuff ring (Sohn et al. 2002; Sohn et al. 2015). The topographic contours are in meters

Songaksan is the youngest volcanic center on Jeju Island, located at the southwestern margin of the island. It comprises a tuff ring with a nested scoria cone and a ponded trachybasalt lava inside the crater (Chough and Sohn 1990; Sohn et al. 2002) (Fig. 1c). The tuff ring is virtually unlithified and was severely eroded by the action of the sea, losing the original "ring" morphology but exposing the cross section of the whole tuff sequence from inside the crater to the distal margin, whereas the nested scoria cones and ponded lava form a promontory because of their resistance to erosion. The tuff ring accumulated upon the Late Pleistocene Kwanghaeak Basalt, which is a pahoehoe lava field forming an extensive and low-altitude coastal plain near sea level in southwestern Jeju Island. The basal few meters of the tuff ring were deposited in the intertidal region with a tidal range less than 2 m, whereas the rest were deposited above sea level (Yoon et al. 2016). The standing body of seawater is therefore interpreted to have played only a minor role in hydrovolcanic explosions because influx of seawater directly into the vent must have been immediately dammed by the construction of the tephra ring around the vent (Chough and Sohn 1990). The tuff sequence thins rapidly from ca. 80 m near the crater rim to <10 cm in a few kilometers (Fig. 2a). Geochemical investigation of tephra suggests that the volcano was produced by multiple magma batches, which erupted sequentially from the same vent (Brenna et al. 2011). Radiocarbon dating of mollusk shells from the basal part of the tuff ring and the organic materials within the paleosol beneath the tuff ring gave an age between 3720 ± 50 and 4130 ± 60 years BP and an age of 3640 ± 50 years BP, respectively (Ahn et al. 2015; Sohn et al. 2015).

The Songaksan tuff ring can be divided into four tuff units (unit A to D from base to top) based on color and componentry of the tuff: dark gray or black and accidental quartz-poor units A and C and olive gray and accidental quartz-rich units B and D. The contacts between these tuff units are sharp and non-erosional (Fig. 2b, c), suggesting deposition of tephra without a break in eruption. A set of

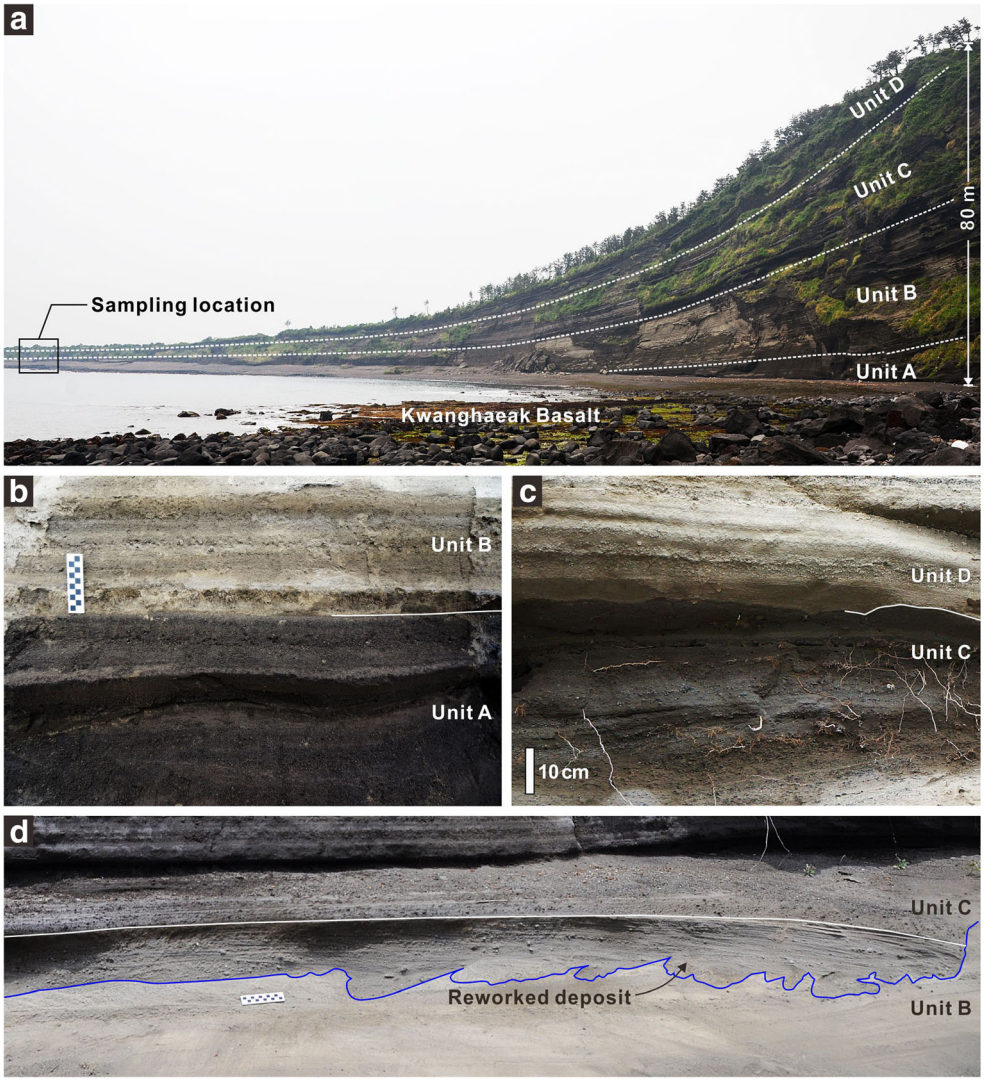

Fig. 2 **a** The exposure of the Songaksan tuff ring along the western coast. The tuff sequence can be divided into four tuff units based on tuff color and componentry. It is 80 m thick at the crater rim and thins exponentially away from the rim. **b**, **c** The sharp and non-erosional contacts between dark gray tuffs of units A and C and olive gray tuffs of units B and D. The depositional features of the tuff units indicate deposition mainly from moist pyroclastic surges. **d** Erosional contact between units B and C with an intercalation of low-angle cross-stratified deposit, which is interpreted to represent a storm event during the eruption of Songaksan (Sohn and Sohn 2016). The photo scales in **b** and **d** are graduated in centimeters

prominent erosion surfaces are found along the contact between units B and C (Fig. 2d). The erosion surfaces do not imply a break in eruption but are interpreted to record a storm event during the eruption of Songaksan (Sohn and Sohn 2016). The whole tuff ring is therefore interpreted to have resulted from a single continuous eruption.

The relative proportions of fall deposits, which occur mostly as thin (less than a few centimeters thick), continuous fine ash layers with uniform thicknesses over undulating bedforms or bedding sag depressions and commonly contain abundant accretionary lapilli, are estimated to be a few to 10% in thickness in units B, C, and D (Chough and Sohn 1990). The relative proportion of fall deposits in unit A is as much as about 20% in thickness (Yoon et al. 2016). The four tuff units are also identified in the tuff sequence exposed along the northeastern coast of Songaksan with similar thicknesses. This suggests that the ejecta was almost symmetrically dispersed around the crater of the tuff ring and that the tuff samples taken from the western coast of the tuff ring (Fig. 1c) can represent the whole tuff sequence of Songaksan. An exposure along the northeastern coast also shows that the tuff units have the virtually identical deposit facies and inferred depositional processes in spite of the distinct contrasts in tuff colors and componentry (Fig. 3), which reflect different eruptive conditions in the diatreme, as will be discussed later.

Substrate characteristics

More than 5000 groundwater wells have been drilled all over Jeju Island since the 1960s, revealing the details of the subsurface stratigraphy, lithology, and groundwater hydrology of the island (Hahn et al. 1997; Koh 1997; Sohn and Park 2004; Won et al. 2005; Koh et al. 2006; Won et al. 2006; Sohn et al. 2008; Koh et al. 2013; Mair et al. 2013) (Fig. 4a). The basement rocks are first encountered ca. 150 to 310 m below sea level in the boreholes and comprise Jurassic and Cretaceous granites in the majority of the island. In the eastern part, however, the basement comprises Cretaceous silicic (rhyolitic to

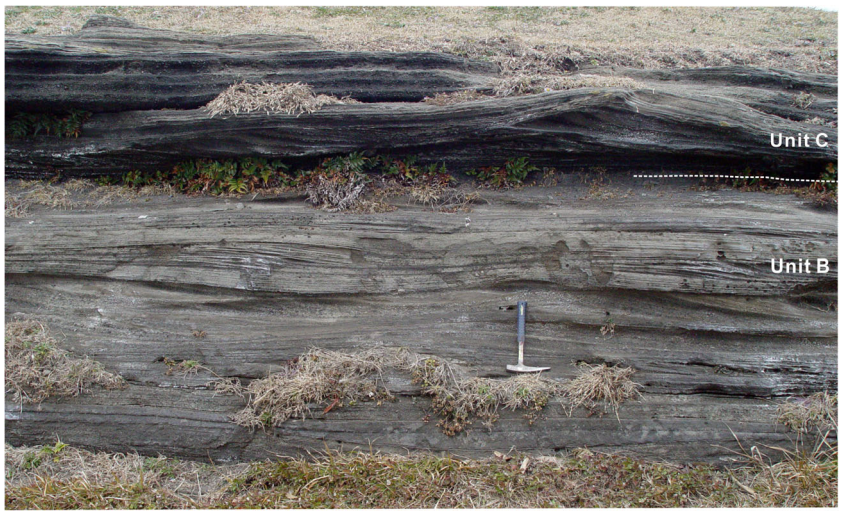

Fig. 3 An exposure of units B and C along the eastern coast of Songaksan, showing different tuff colors but identical deposit facies. See Fig. 1 for the location of the photograph

dacitic) volcanic and volcaniclastic rocks. In the western to southwestern part, including the Songaksan area, the basement consists of quartzose sedimentary rocks of unknown age (Fig. 4b, c).

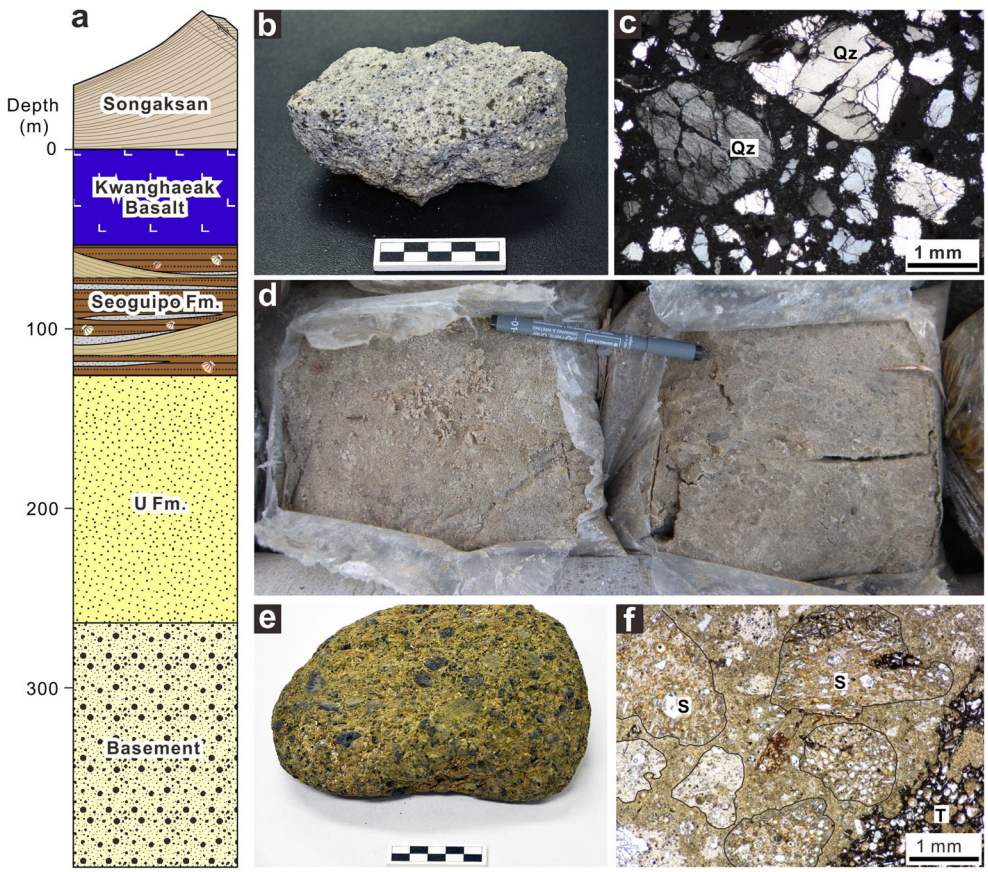

Fig. 4 **a** Schematic column of the subsurface stratigraphic units beneath Songaksan compiled from a number of borehole data sources, including Koh (1997), Sohn et al. (2008), Koh et al. (2013), and many unpublished reports of the Korea Agricultural Corporation and Water Industry Research Center of Jeju Special Self-Governing Province Development Corporation. **b** A quartzose sedimentary rock fragment from the proximal part of the Songaksan tuff ring. **c** Thin-section photomicrograph of a quartzose sedimentary rock fragment under crossed nicols, dominantly comprising fractured quartz grains (Qz). **d** Well-sorted quartz sand of the U Formation from a borehole located in the southeastern part of Jeju Island. The sediments of the U Formation are only rarely recovered as cores because of their unconsolidated and uncemented nature. **e** A basaltic lapilli tuff fragment from the proximal part of the Songaksan tuff ring, consisting of black basaltic lapilli set in a yellowish palagonitized ash matrix. **f** Thin-section photomicrograph of a basaltic tuff clast under open nicols, consisting of sideromelane (S) and tachylite (T) grains in a poorly sorted fine ash matrix. The photo scales in **b** and **e** are graduated in centimeters. The pen for scale in *d* is 13 cm long

Above the basement lies a sequence of unconsolidated quartzose sand and mud, named the U Formation (Koh 1997) (Fig. 4d). The formation is 150 m thick on average, and its upper surface is encountered ca. 120 m below sea level in the boreholes, approximately identical to the seafloor depth around Jeju Island. The formation contains calcareous marine nanofossils and is interpreted to have accumulated on the continental shelf in the Pliocene before the onset of volcanism in the Jeju Island area (Sohn and Park 2004).

The Seoguipo Formation above the U Formation is the product of hydrovolcanic activity on the continental shelf between ca. 1.8 and 0.5 Ma (Fig. 4e, f). Detailed sedimentological analysis of some cores (Sohn et al. 2008) reveals that the formation comprises numerous superposed phreatomagmatic volcanoes (tuff rings and tuff cones) and intercalated marine or non-marine, volcaniclastic, and rare non-volcaniclastic deposits, recording the widespread and continual hydrovolcanic activity and associated volcaniclastic sedimentation under the influence of fluctuating Quaternary sea levels. Borehole drilling reveals that the average thickness of the formation is 64 m and that the upper surface of the formation is encountered ca. 50–60 m below sea level in the western part, ca. 110 m below sea level in the eastern part, and ca. 200 m above sea level in the central part of Jeju Island. Some volcanic edifices belonging to the Seoguipo Formation protrude above the overlying lavas (Sohn and Park 2005). The lavas are only 50 to 60 m thick in the western and southwestern margins of Jeju Island and consists of thin, pahoehoe to aa lavas intercalated with clinker, scoria, and paleosol layers (Jeon et al. 2013).

To summarize, the Songaksan volcano is interpreted to be underlain by ca. 50–60-m-thick lavas, ca. 60–70-m-thick basaltic volcaniclastic deposits of the Seoguipo Formation, ca. 150-m-thick quartzose sand and mud of the U Formation, and then the quartzose basement rocks (Fig. 4a). The volcaniclastic deposits of the Seoguipo Formation are variably lithified. The core specimens can thus be easily broken or crushed with hands, depending on the degree of palagonitization of tuff and the sorting or fine ash matrix content of the deposits. The quartzose sand and mud of the U Formation are unconsolidated and uncemented. The quartzose sands of the U Formation are especially well sorted and as loose as modern sand (Fig. 4d), probably because of their deposition in the tidal sand ridges that cover the seafloor of the Yellow Sea continental shelf (Shinn et al. 2007) and because of the lack of any cementing materials and clayey matrix in the interstices (Koh 1997; Jeong et al. 2016). The quartzose basement rocks are also porous and so fragile that they can be easily broken or crushed with hands.

The substrate stratigraphy and lithology of Jeju Island thus provides a peculiar condition for phreatomagmatic eruption and diatreme formation of Songaksan in that the most rigid strata (the lavas) occur at the top, the less rigid strata (the Seoguipo Formation) occur beneath it, and the most fragile strata (the U Formation) occur further below. We hypothesize that the inverted rigidity profile might have affected significantly the geometry of the diatreme beneath Songaksan. It is also worth noting that the basement did not act as the lower limit of magma-water interaction and downward diatreme excavation because of its porous and fragile nature.

Materials and methods

The Songaksan tuff ring is composed dominantly of tuff, with lapilli tuff restricted mainly to the proximal part. Blocks are present as isolated clasts in the proximal-to-medial deposits but never form a continuous layer. The overall componentry of the Songaksan tuff ring thus appears to be represented by tuffs rather than by coarser grained deposits. A total of 30 samples were collected from a medial-to-distal location, ca. 850 to 900 m away from the center of the tuff ring (Figs. 1c and 2a), where the sampling of the whole sequence, about 8.5 m thick, was possible, although unit D was partly removed by erosion in the upper part. The deposits here comprise mostly thin-bedded and well-bedded tuffs with downcurrent-migrating climbing megaripple bedforms, downcurrent-migrating low-relief undulations, and plane-parallel to mantle bedding (Fig. 5). Accretionary or armored lapilli are commonly scattered within beds or occur in diffuse layers. These features indicate that all these units were emplaced by dilute and moist pyroclastic density currents (surges) and associated fallout (Chough and Sohn 1990).

The average bulk density and porosity of the Songaksan tuffs were measured to be 1.65 g/cm^3 and 34.7%, respectively (Sohn 2015). The point compressive strength of the tuffs measured by the point load strength test (Broch and Franklin 1972) is 31.5 kgf/cm^2 (=3.1 MPa) on average, indicating that the tuffs belong to "very weak rock" according to the classification scheme of Brown (1981). The average vesicularity of juvenile tephra is calculated to be 8% based on the density and porosity data from the tuffs.

Samples weighting a few hundred grams were taken with a trowel from 30 horizons of the tuff sequence (Fig. 5). The tuffs were mostly disintegrated into grains during sampling and transportation to the laboratory. About a hundred grams of each sample was separated with a sediment splitter for grain size and componentry analyses. The samples were then immersed in water for a day and treated in an ultrasonic vibrator for 10 min in order to clean the surface of the tephra grains and make the observations of grain surface features easier, rather than to further disintegrate the samples, because they were

Fig. 5 Graphic column of the tuff sequence in the medial-distal part of the Songaksan tuff ring with sample locations. Histograms on the right show the componentry and grain size distribution in each sample. Extremely fine ash (<4 Φ) and very coarse ash to lapilli (>0 Φ) were excluded from the componentry analysis and are shown by *black bars* on the histograms. ▶

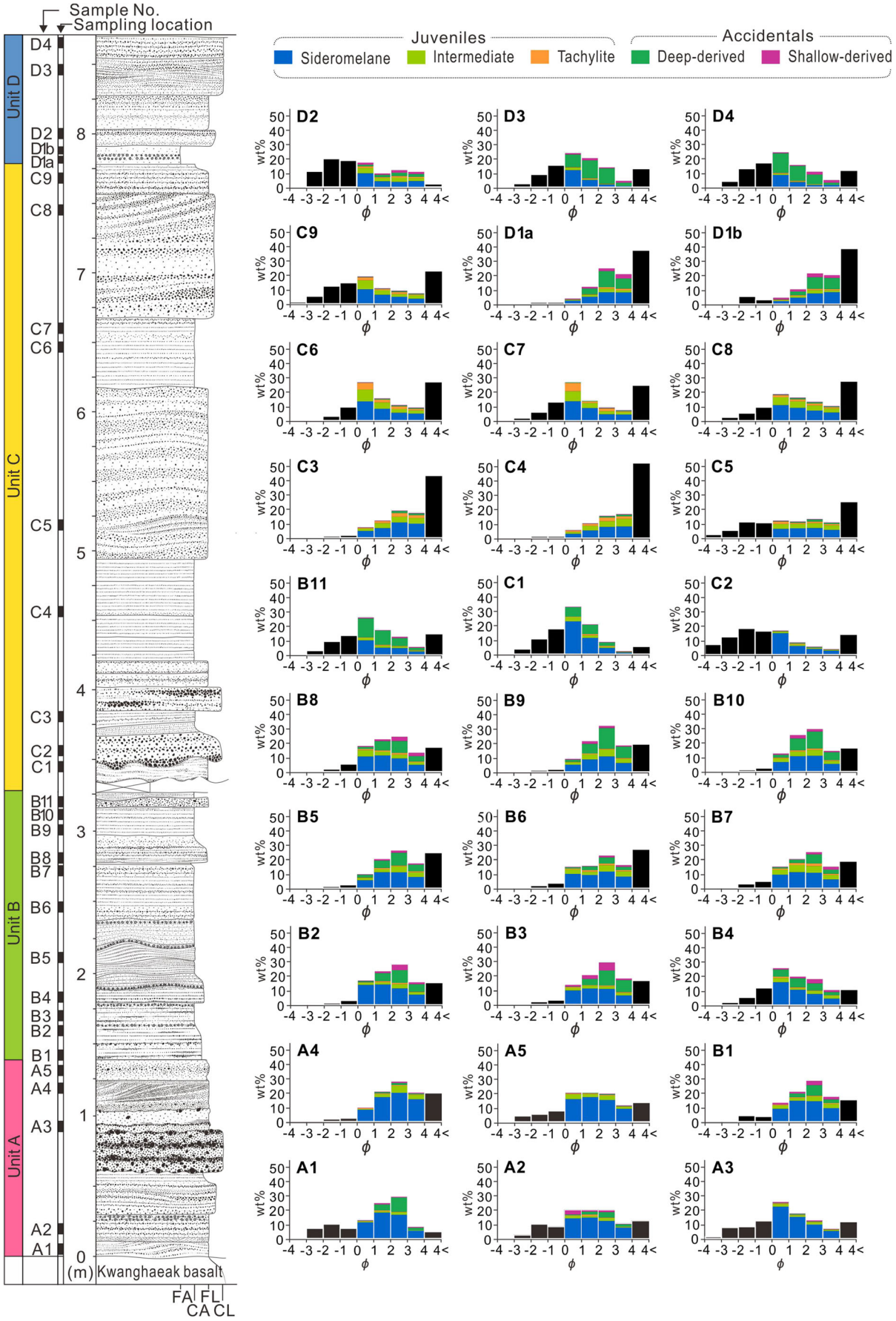
Sample No.
Sampling location
Unit D
Unit C
Unit B
Unit A
D4
D3
D2
D1b
D1a
C9
C8
C7
C6
C5
C4
C3
C2
C1
B11
B10
B9
B8
B7
B6
B5
B4
B3
B2
B1
A5
A4
A3
A2
A1
0
1
2
3
4
5
6
7
8
(m)
Kwanghaeak basalt
FA
FL
CA
CL
Juveniles
Sideromelane
Intermediate
Tachylite
Accidentals
Deep-derived
Shallow-derived
wt%
ϕ
D2
D3
D4
C9
D1a
D1b
C6
C7
C8
C3
C4
C5
B11
C1
C2
B8
B9
B10
B5
B6
B7
B2
B3
B4
A4
A5
B1
A1
A2
A3

already mostly disintegrated into grains before immersion into water. Ash lumps and aggregates that were left in some samples after this procedure were so fragile that they could not be removed by picking up with fingers or tweezers and were disintegrated by lightly pressing down them with fingers. They were then dried and weighed to get the total weight. Those fractions coarser than 4 Φ (1/16 mm) were then selected by wet sieving, dried, dry-sieved at 1 Φ interval, and weighed, following the standard procedure for grain size analysis (Carver 1971) (Table 1). The fractions finer than 4 Φ were not processed for further analysis but were assumed to comprise mostly silt-size grains between 4 and 9 Φ (Fig. 5). Grain size parameters were then calculated by the inclusive graphics method of Folk (1974) using a software provided by the US Geological Survey (Poppe et al. 2004). The analysis shows that most samples belong to the "tuff" field of Fisher (1966), containing less than 25% lapilli. The mode was at the 2–3 Φ interval (fine ash; terminology of White and Houghton 2006) for 16 samples and at the 0–1 Φ interval (coarse ash) for 12 samples (Table 1). Interestingly, no samples had a mode at the 1–2 Φ interval (medium ash).

The ash grains of each size fraction between 0 Φ (1 mm) and 4 Φ (1/16 mm) from the 30 samples were then impregnated with epoxy and prepared for 120 polished thin sections for componentry analysis and other observations. Very coarse ash-sized to lapilli-sized grains coarser than 0 Φ (1 mm) were excluded from this procedure because most samples comprised only a few lapilli grains, and the amount of very coarse ash was insufficient to make a polished section for most samples (Table 1). These grains were thus observed only under an

Table 1 Results of grain size analysis of the Songaksan tuff samples

Sample no.	Weight %									Md	M	σ	Sk
	−4/−3	−3/−2	−2/−1	−1/0	0/1	1/2	2/3	3/4	4<				
A1	0.00	6.89	9.65	6.37	12.50	23.93	28.64	7.68	4.34	1.65	1.13	1.89	−0.34
A2	0.00	1.78	9.51	7.79	19.48	19.33	19.69	10.37	12.05	1.59	1.6	1.97	0.02
A3	0.90	6.94	7.88	11.95	25.21	16.61	12.30	6.71	11.50	0.87	1.06	2.17	0.13
A4	0.00	0.00	1.56	1.77	9.75	20.80	27.45	19.20	19.48	2.58	2.66	1.54	0.09
A5	0.00	3.64	5.16	7.27	20.16	20.09	19.44	11.22	13.02	1.68	1.79	1.95	0.05
B1	0.00	0.00	3.75	3.19	12.68	20.45	28.08	17.11	14.73	2.36	2.35	1.66	0
B2	0.00	0.00	0.45	2.54	16.35	22.77	27.69	15.50	14.70	2.28	2.34	1.53	0.12
B3	0.00	0.00	1.64	2.60	12.86	20.05	29.12	17.66	16.06	2.44	2.46	1.56	0.06
B4	0.00	1.26	4.70	11.60	25.24	19.25	17.63	9.89	10.43	1.35	1.54	1.77	0.17
B5	0.00	0.00	0.85	1.95	9.84	20.14	25.85	17.38	23.98	2.65	2.79	1.64	0.13
B6	0.00	0.00	1.39	3.25	14.63	15.59	22.38	16.14	26.61	2.67	2.7	1.82	0.05
B7	0.00	0.00	2.62	4.45	14.78	20.27	24.67	14.98	18.23	2.32	2.39	1.76	0.07
B8	0.00	0.00	1.50	4.58	17.87	22.35	24.04	12.97	16.69	2.15	2.28	1.69	0.14
B9	0.00	0.00	0.11	1.09	8.95	21.15	31.59	18.29	18.82	2.57	2.7	1.43	0.15
B10	0.00	0.00	0.56	1.82	12.75	25.27	29.29	14.11	16.19	2.31	2.46	1.5	0.17
B11	0.00	2.57	9.04	13.01	25.93	17.31	12.45	5.33	14.36	0.97	1.35	2.12	0.25
C1	0.00	3.03	10.40	17.28	33.15	20.54	8.64	1.90	5.06	0.58	0.58	1.57	0.1
C2	6.80	11.65	17.50	16.01	16.66	8.48	5.74	3.61	13.56	−0.12	0.34	2.63	0.25
C3	0.00	0.00	0.46	1.41	7.29	11.67	19.10	17.37	42.70	3.6	3.43	1.69	−0.13
C4	0.00	0.00	0.11	0.77	5.53	9.86	15.64	16.32	51.76	4.08	3.84	1.71	−0.19
C5	1.89	4.61	11.00	10.16	11.92	11.59	13.16	10.66	25.01	1.9	1.78	2.63	−0.05
C6	0.00	0.00	2.29	9.07	26.46	15.71	10.85	8.80	26.82	1.74	2.21	2.07	0.26
C7	0.00	1.28	5.32	12.55	26.79	13.57	9.27	7.12	24.11	1.24	1.87	2.22	0.34
C8	0.00	1.73	4.74	8.76	18.27	15.90	13.28	10.32	27.00	2.04	2.34	2.29	0.13
C9	0.43	4.86	12.07	14.05	18.91	10.53	8.91	7.51	22.73	0.98	1.44	2.52	0.22
D1a	0.00	0.00	0.69	0.76	3.59	11.92	25.09	20.55	37.40	3.37	3.46	1.55	0.07
D1b	0.00	0.00	4.77	2.39	4.07	10.09	21.41	19.19	38.07	3.37	3.35	1.94	−0.13
D2	0.00	10.48	19.71	18.38	17.42	9.61	11.76	10.60	2.05	0.08	0.37	2.02	0.18
D3	0.00	2.19	8.57	14.70	23.53	20.11	13.60	4.57	12.73	1.05	1.23	1.96	0.18
D4	0.00	3.44	12.56	16.46	24.38	15.42	11.03	5.11	11.60	0.7	0.93	2.06	0.22

Md median (Φ), *M* mean (Φ), *σ* standard deviation (Φ), *Sk* skewness

optical microscope and excluded from the statistical summation of the componentry. Backscattered electron (BSE) images were obtained from the polished sections using a JEOL JXA-8100 electron microprobe in the Center for Research Facilities of Gyeongsang National University. About 500 ash grains were observed and counted from the BSE images of each polished section in order to distinguish between their grain componentry (juvenile vs. accidental), surface textures (ash-coated vs. uncoated), and internal textures (sideromelane vs. tachylite) (Table 2). Observations using a JEOL JSM-7610F field emission scanning electron microscope in addition to an optical stereoscopic microscope were made for selected juvenile grains in the 2–3 Φ interval to see the surface morphology and other microscopic features of the tephra grains. The chemical composition of the microlite-free glass of 2 to 3 juvenile grains from most samples and 9 to 10 grains from samples B11, C1, and C2

Table 2 Results of grain componentry analysis of the Songaksan tuff samples

Sample no.	Juveniles (%)				Accidentals (%)				
	S	*I*	*T*	Total	Shallow-derived		Deep-derived		Total
					Blt	SGF	Qz	Acc	
A1	67.0	4.7	1.3	73.1	0.1	2.0	20.3	4.6	26.9
A2	68.7	8.0	2.5	79.2	0.1	6.7	12.1	1.9	20.8
A3	83.9	9.4	2.5	95.8	0.1	1.6	2.2	0.3	4.2
A4	77.7	13.2	2.8	93.7	0.0	1.7	3.8	0.8	6.3
A5	80.6	14.9	2.3	97.8	0.0	0.7	1.4	0.1	2.2
$A_{average}$	75.6	10.0	2.3	87.9	0.0	2.5	7.9	1.6	12.1
B1	58.0	13.2	3.2	74.5	0.1	5.8	16.1	3.6	25.5
B2	53.7	9.6	2.9	66.3	0.1	5.5	23.8	4.3	33.7
B3	45.0	9.2	2.3	56.4	0.3	7.9	28.1	7.2	43.6
B4	50.8	11.5	3.0	65.2	0.5	5.1	26.2	2.9	34.8
B5	46.9	15.2	3.8	65.9	0.2	3.2	27.0	3.7	34.1
B6	55.0	20.4	5.6	80.9	0.2	2.1	14.0	2.7	19.1
B7	48.4	22.6	6.4	77.3	0.3	3.4	16.3	2.6	22.7
B8	44.5	14.8	4.1	63.5	0.2	5.8	26.7	3.8	36.5
B9	36.1	15.9	3.1	55.1	0.1	5.7	33.5	5.7	44.9
B10	39.3	15.1	3.7	58.1	0.5	5.8	29.8	5.9	41.9
B11	33.7	8.3	2.4	44.4	0.6	0.6	51.4	3.0	55.6
$B_{average}$	46.5	14.2	3.7	64.3	0.3	4.6	26.6	4.1	35.7
C1	59.8	9.9	2.5	72.2	0.2	0.5	25.7	1.3	27.8
C2	80.4	10.2	3.3	93.9	0.0	0.3	5.3	0.5	6.1
C3	56.8	24.9	11.9	93.6	0.1	0.5	4.7	1.1	6.4
C4	48.9	30.3	14.3	93.4	0.3	0.2	4.8	1.3	6.6
C5	52.5	29.0	10.1	91.5	0.4	0.9	6.1	1.1	8.5
C6	50.4	29.5	16.4	96.4	0.2	0.3	2.7	0.4	3.6
C7	53.4	25.7	17.6	96.7	0.0	0.2	2.8	0.4	3.3
C8	55.1	30.0	9.5	94.6	0.2	0.3	4.3	0.7	5.4
C9	53.0	32.0	10.3	95.3	0.2	0.5	3.6	0.4	4.7
$C_{average}$	56.7	24.6	10.6	92.0	0.2	0.4	6.7	0.8	8.0
D1a	35.7	10.0	4.3	50.0	0.2	8.8	34.8	6.2	50.0
D1b	37.3	9.5	4.3	51.1	0.1	10.8	32.4	5.6	48.9
D2	43.4	21.9	8.3	73.6	0.3	8.5	15.8	1.8	26.4
D3	28.9	4.4	1.9	35.3	0.1	5.1	54.8	4.9	64.9
D4	24.7	3.0	2.2	30.1	0.2	7.5	59.4	2.9	70.0
$D_{average}$	34.0	9.8	4.2	48.0	0.2	8.1	39.4	4.3	52.0

S sideromelane, *I* intermediate, *T* tachylite, *Blt* crystalline basalt fragment, *SGF* tuff fragments and palagonitized grains, *Qz* quartz grains and quartzose rock fragments, *Acc* accessory mineral grains (K-feldspar, mica, heavy minerals, and etc.)

was obtained using a JEOL JXA-8100 wavelength dispersive electron microprobe with ZAF matrix correction in the same institute (Table 3). The microprobe was operated with an accelerating voltage of 15 kV, beam current of 10 nA, beam diameter of 1 μm, peak counting time of 20 s, and background counting time of 10 s. Natural minerals were used as standards for Na, Si, Fe, K, Al, Mn, Ca, Mg, P, Cr, and Ti. Accidental lithic clasts were collected from the proximal part of the tuff ring. Thin sections were then prepared for these clasts for petrographic observations and comparison with the subsurface stratigraphic units.

Results

Juvenile grains

Juvenile grains are generally angular and blocky in shape with irregular margins. They are variably vesicular but generally incipiently vesicular to non-vesicular (terminology of Houghton and Wilson 1989) and contain variable amounts of euhedral to subhedral crystals of plagioclase, olivine, pyroxene, spinel, and magnetite in a glassy groundmass. They are classified into three types: sideromelane, tachylite, and intermediate grains, based mainly on the distribution density of Fe-oxide microlites on the BSE images (Fig. 6). The sideromelane grains are composed of colorless to light yellow glass under optical microscope and pristine glass on the BSE images with scarce Fe-oxide microlites and relatively rare and small plagioclase laths (Fig. 6a). On the other hand, the tachylite grains have an opaque groundmass under optical microscope and densely populated microlites of Fe oxides that surround or coat the plagioclase laths on BSE images. Plagioclase laths are generally more abundant and larger than those in the sideromelane grains (Fig. 6c). The intermediate grains have intermediate amounts of Fe-oxide microlites, which commonly occur as thin coatings on plagioclase or olivine crystals. They are dark brown and translucent under optical microscope (Fig. 6b). There is also a tendency for the vesicles to be more spherical in the sideromelane grains and more irregular in the tachylite grains.

Accidental grains

Five types of accidental grains are identified in the medial-distal tuff beds of Songaksan, including (1) crystalline basalt fragments (Fig. 7a), (2) basaltic tuff fragments (Fig. 7b), (3) monocrystalline quartz grains (Fig. 7c), (4) polycrystalline quartz grains or quartzose rock fragments (Fig. 7d), and (5) accessory mineral grains, such as alkali feldspar, mica, and heavy minerals (Fig. 7e). The crystalline basalt fragments contain abundant olivine and plagioclase phenocrysts in a microcrystalline groundmass rich in plagioclase laths. Some fragments contain irregular vesicles. They are interpreted to have been derived mainly from the underlying lavas, although some might have been derived from disintegrated intradiatreme dikes (White and Ross 2011). The basaltic tuff fragments consist of dark colored, ash-sized to lapilli-sized and generally non-vesicular basaltic grains set in a brownish to yellowish matrix (Fig. 4e). Under the microscope, they are identified as either transparent sideromelane or opaque tachylite (Fig. 4f) commonly with alteration or palagonitized rims along the grain margins and vesicle walls (Fig. 7b). These features indicate that they were derived from the basaltic volcaniclastic deposits of the Seoguipo Formation. The monocrystalline quartz grains are the most abundant accidental materials in the tuff ring. They are generally angular and rarely have partially preserved quartz overgrowth along the grain margins (Fig. 7c), suggesting their origin from sedimentary rocks. They are interpreted to have been derived mainly from the sand deposits of the U Formation and subordinately from the quartzose basement rocks. Minor amounts of quartz grains might have originated from the Seoguipo Formation because some of the volcaniclastic deposits of the formation contain accidental quartz grains. The polycrystalline quartz grains and quartzose rock fragments show pervasive internal fractures and secondary pores (Figs. 4c and 7d). They are interpreted to have been derived from the quartzose basement rocks. The accessory mineral grains of alkali feldspar, mica, and heavy minerals are also interpreted to have been derived from the basement rocks.

We use the term “deep-derived” for the quartzose rock fragments and the quartz and accessory mineral grains that were derived mostly from the U Formation and the underlying basement rocks and the term “shallow-derived” for the crystalline basalt and the tuff fragments that were derived from the lavas and the underlying Seoguipo Formation when describing the accidental componentry, because they were derived from the relatively deeper (>120 m) and shallower (<120 m) levels of the substrate, respectively. It should be noted that some of the materials derived from the Seoguipo Formation might have been counted as juvenile grains because some deposits of the formation are poorly lithified and might have provided unaltered basaltic ash grains to the erupting materials upon disintegration. We found that the basaltic grains from the Seoguipo Formation contain amphibole phenocrysts in some cases and have lower SiO_2 and higher alkali contents than the Songaksan tuff. However, these differences could not be taken into account during the counting of ca. 60,000 grains on the polished sections. On the other hand, some juvenile ash aggregates or accretionary lapilli that survived the procedures for grain disintegration during sample preparation might have been counted as accidental tuff fragments from the Seoguipo Formation. All quartzose grains are regarded to be deep-derived although some quartz grains might have originated from the volcaniclastic deposits of the Seoguipo Formation. Crystalline basalt

Table 3 Major element composition of glassy groundmass of sideromelane grains in the Songaksan tuff samples

Sample no.	SiO_2	TiO_2	Al_2O_3	FeO*	Cr_2O_3	MnO	MgO	CaO	Na_2O	K_2O	P_2O_5	Total	Mg#
A1-1	51.15	3.32	14.76	11.64	0.00	0.19	3.66	7.70	3.56	2.14	0.77	98.86	38.8
A1-2	50.83	3.32	14.71	11.08	0.00	0.12	3.69	7.61	4.05	2.15	0.66	98.21	40.2
A1-3	51.42	3.23	14.56	11.11	0.03	0.19	3.65	7.44	3.45	2.14	0.61	97.82	39.9
A2-1	52.34	3.26	14.69	10.84	0.00	0.22	3.21	6.80	3.64	2.43	0.76	98.20	37.4
A2-2	51.92	3.15	14.87	11.08	0.04	0.20	3.44	7.05	2.98	2.26	0.63	97.61	38.5
A2-3	52.51	3.02	15.02	10.99	0.00	0.19	3.38	7.04	3.04	2.14	0.67	97.99	38.3
A3-1	52.46	2.69	15.25	10.82	0.00	0.19	3.21	6.48	3.53	2.15	0.68	97.43	37.5
A3-2	52.58	2.94	15.32	10.40	0.01	0.17	2.97	6.77	3.75	2.47	0.68	98.06	36.6
A4-1	52.90	2.47	16.65	9.74	0.00	0.14	3.15	7.08	3.52	2.40	0.71	98.76	39.5
A4-2	52.66	2.56	16.65	9.93	0.00	0.17	3.02	6.81	3.87	2.42	0.61	98.70	38.0
A5-1	52.56	2.88	15.37	10.06	0.03	0.18	3.27	6.56	3.42	2.39	0.63	97.34	39.6
A5-2	51.89	3.07	14.71	11.01	0.00	0.21	3.26	6.99	3.45	2.75	0.57	97.89	37.4
B1-1	53.03	2.88	15.58	9.90	0.00	0.19	3.29	6.55	3.84	2.19	0.84	98.29	40.2
B1-2	53.36	2.84	14.94	10.83	0.00	0.16	3.18	6.47	3.79	2.69	0.82	99.07	37.2
B2-1	53.01	3.02	15.20	10.10	0.02	0.18	2.83	6.44	3.36	2.57	0.47	97.20	36.1
B2-2	53.21	3.07	14.93	10.05	0.00	0.21	3.15	6.71	3.66	2.40	0.66	98.03	38.8
B3-1	51.68	3.10	15.06	10.73	0.02	0.18	3.33	6.81	2.25	3.72	0.80	97.69	38.5
B3-2	52.72	2.89	15.18	10.48	0.00	0.17	3.09	6.30	3.68	2.60	0.75	97.84	37.3
B4-1	53.32	3.00	14.81	10.53	0.02	0.18	3.11	6.32	3.57	2.49	0.73	98.08	37.4
B4-2	52.47	2.89	15.00	10.50	0.00	0.15	3.06	6.63	3.77	2.53	0.75	97.73	37.0
B4-3	53.16	3.08	15.13	10.48	0.02	0.14	3.05	6.48	3.48	2.75	0.84	98.60	37.0
B5-1	53.01	3.02	15.20	10.10	0.02	0.18	2.83	6.44	3.36	2.57	0.47	97.20	36.1
B5-2	53.41	2.95	14.93	10.51	0.00	0.13	3.04	6.17	3.59	2.55	0.71	97.99	36.9
B5-3	53.37	2.85	14.98	10.91	0.05	0.18	3.02	6.62	3.50	2.58	0.67	98.73	35.9
B6-1	52.31	2.87	15.29	10.63	0.00	0.18	3.08	6.66	3.22	2.54	0.70	97.48	36.9
B6-2	51.67	3.23	14.23	10.90	0.00	0.17	3.15	6.79	3.07	2.68	0.65	96.52	36.9
B7-1	52.41	3.02	14.93	10.38	0.00	0.17	3.25	6.53	3.57	2.44	0.73	97.42	38.7
B7-2	52.72	2.95	15.37	10.37	0.02	0.20	3.20	6.60	3.38	2.50	0.69	98.00	38.4
B8-1	52.59	3.03	15.03	10.68	0.00	0.15	3.20	6.30	3.62	2.48	0.75	97.83	37.7
B8-2	52.21	2.80	15.51	10.52	0.01	0.16	3.32	6.96	3.93	2.30	0.77	98.50	38.9
B9-1	52.09	2.82	15.27	10.37	0.00	0.17	3.27	6.67	3.61	2.34	0.58	97.18	38.9
B9-2	52.24	3.19	14.77	11.09	0.00	0.17	3.17	6.78	3.49	2.45	0.71	98.04	36.6
B10-1	51.19	2.56	16.75	10.44	0.03	0.15	3.07	7.31	3.93	2.25	0.46	98.13	37.3
B10-2	52.14	2.98	15.16	10.40	0.00	0.15	3.26	6.41	3.56	2.42	0.57	97.05	38.8
B10-3	52.11	2.59	15.34	10.15	0.02	0.21	2.94	6.63	3.24	2.52	0.47	96.23	36.9
B11-1	51.40	2.55	15.22	10.54	0.01	0.18	3.66	7.27	3.71	2.13	0.56	97.22	41.2
B11-2	50.74	2.54	15.14	10.69	0.03	0.12	4.36	8.59	3.63	1.79	0.37	98.00	45.2
B11-3	50.51	2.54	15.19	10.47	0.04	0.21	4.30	8.48	3.70	1.74	0.48	97.65	45.3
B11-4	50.96	2.88	15.29	10.43	0.04	0.15	4.01	8.49	4.08	1.70	0.36	98.39	43.7
B11-5	51.61	2.95	15.47	10.56	0.06	0.15	3.49	7.73	4.17	2.07	0.36	98.62	40.0
B11-6	51.58	2.82	15.7	10.33	0.00	0.16	3.43	7.34	4.13	2.07	0.38	97.93	40.1
B11-7	52.45	2.83	15.87	10.34	0.00	0.13	3.02	6.63	4.53	2.24	0.79	98.84	35.4
B11-8	53.09	2.88	15.54	10.25	0.03	0.21	2.91	6.36	4.54	2.55	0.62	98.97	36.4
B11-9	51.67	2.92	15.64	10.53	0.00	0.21	3.29	7.08	4.18	2.20	0.53	98.24	38.7
C1-1	50.19	2.69	15.32	9.91	0.01	0.11	4.50	8.62	3.78	1.62	0.40	97.15	47.8
C1-2	50.86	2.61	15.59	10.16	0.01	0.15	4.66	8.71	3.73	1.70	0.44	98.61	48.1
C1-3	51.19	2.45	15.81	9.93	0.02	0.16	4.64	8.51	3.53	1.93	0.54	98.71	48.5
C1-4	50.44	2.52	16.09	9.63	0.04	0.14	4.36	8.71	4.04	1.61	0.23	97.78	47.8
C1-5	50.60	2.58	16.3	10.01	0.03	0.17	4.25	8.94	3.68	1.50	0.41	98.48	46.2

Table 3 (continued)

Sample no.	SiO_2	TiO_2	Al_2O_3	FeO*	Cr_2O_3	MnO	MgO	CaO	Na_2O	K_2O	P_2O_5	Total	Mg#
C1-6	50.42	2.66	15.57	10.3	0.00	0.17	4.24	8.55	4.02	1.66	0.39	98.16	38.7
C1-7	50.64	2.54	16.13	9.84	0.01	0.17	4.29	8.72	3.78	1.68	0.37	98.17	46.8
C1-8	50.64	2.63	15.59	10.28	0.02	0.14	4.29	8.75	3.81	1.62	0.26	98.05	45.7
C1-9	50.47	2.62	15.73	9.98	0.01	0.15	4.39	8.83	3.86	1.60	0.44	98.05	45.7
C1-10	50.38	2.59	15.61	10.17	0.00	0.08	4.50	8.67	3.90	1.69	0.20	97.79	47.2
C2-1	50.67	2.54	15.82	9.83	0.01	0.15	4.67	8.69	3.87	1.64	0.35	98.26	49.0
C2-2	50.50	2.57	15.85	9.80	0.02	0.13	4.74	8.73	3.70	1.64	0.47	98.15	49.4
C2-3	50.80	2.59	15.82	9.56	0.00	0.13	4.69	8.74	3.52	1.62	0.49	97.95	50.0
C2-4	50.19	2.51	15.99	9.98	0.04	0.19	4.34	8.81	3.91	1.59	0.31	97.85	46.8
C2-5	50.68	2.56	16.22	9.91	0.04	0.16	4.33	8.86	3.91	1.61	0.41	98.69	46.9
C2-6	50.94	2.57	15.7	10.12	0.03	0.12	4.35	8.89	4.00	1.62	0.44	98.77	47.2
C2-7	50.58	2.75	15.58	10.46	0.03	0.18	4.31	8.86	3.93	1.74	0.32	98.74	45.4
C2-8	50.63	2.64	15.99	10.15	0.01	0.14	4.45	8.82	3.84	1.54	0.25	98.47	47.0
C2-9	50.39	2.66	15.46	10.35	0.04	0.20	4.48	8.91	3.91	1.71	0.38	98.47	47.1
C3-1	50.99	2.45	16.69	9.77	0.07	0.18	4.13	9.65	3.81	1.54	0.36	99.64	46.1
C3-2	50.02	2.56	15.66	9.50	0.05	0.13	4.66	8.70	3.48	1.48	0.40	96.64	49.8
C4-1	51.62	2.29	15.89	9.99	0.02	0.13	4.07	6.99	3.65	2.01	0.52	97.18	45.1
C4-2	51.19	2.31	15.91	9.90	0.00	0.16	4.00	6.96	3.22	1.96	0.54	96.15	44.9
C5-1	50.14	2.42	14.89	10.40	0.04	0.15	4.90	8.80	3.30	1.75	0.47	97.26	48.8
C5-2	50.91	2.33	15.64	9.86	0.00	0.15	4.77	8.74	4.02	1.61	0.60	98.62	49.4
C6-1	50.88	2.46	14.76	10.52	0.01	0.14	4.67	8.88	3.35	1.79	0.42	97.88	47.3
C6-2	51.58	2.36	15.70	10.18	0.00	0.12	4.13	7.56	3.74	1.95	0.58	97.89	45.0
C6-3	51.46	2.69	15.41	10.24	0.00	0.17	4.42	8.06	3.56	1.82	0.51	98.32	46.6
C7-1	51.67	2.57	15.89	10.17	0.02	0.15	4.16	7.35	3.81	2.00	0.58	98.37	45.2
C7-2	51.37	2.66	15.72	9.94	0.00	0.17	4.26	7.92	3.93	1.91	0.51	98.38	46.4
C7-3	51.65	2.79	15.61	10.26	0.00	0.16	4.27	7.99	3.53	1.83	0.49	98.58	45.7
C8-1	51.27	2.55	16.27	9.60	0.01	0.14	4.51	8.49	3.87	1.70	0.58	98.98	48.7
C8-2	51.34	2.77	15.52	10.11	0.00	0.14	4.79	8.89	3.77	1.77	0.37	99.47	48.9
C8-3	50.50	2.51	15.75	9.94	0.01	0.18	4.21	8.43	3.68	1.66	0.51	97.37	46.1
C9-1	51.43	2.60	16.15	10.04	0.05	0.16	4.33	7.54	3.68	2.05	0.54	98.59	46.6
C9-2	50.95	2.73	15.68	10.23	0.00	0.16	4.39	8.45	3.61	1.79	0.54	98.52	46.4
D1a-1	51.17	2.65	15.76	10.22	0.00	0.15	3.98	6.17	3.80	2.05	0.56	96.51	44.0
D1a-2	52.16	2.74	15.97	10.11	0.00	0.16	3.82	7.06	3.62	2.06	0.56	98.27	43.3
D1a-3	50.79	2.55	15.48	10.21	0.00	0.14	4.53	8.59	3.56	1.69	0.35	97.90	47.3
D1b-1	52.12	2.52	15.90	10.47	0.00	0.21	3.88	7.02	3.78	2.19	0.57	98.65	42.8
D1b-2	52.28	2.54	15.93	10.41	0.03	0.21	3.91	6.85	3.38	2.06	0.55	98.16	43.1
D2-1	52.06	2.85	15.59	10.53	0.00	0.18	3.77	7.01	3.84	2.23	0.46	98.53	42.0
D2-2	52.27	2.83	15.46	10.44	0.00	0.13	3.73	6.92	3.60	2.27	0.47	98.13	41.9
D2-3	52.23	2.72	15.84	10.70	0.00	0.22	3.94	6.96	3.69	2.22	0.51	99.03	42.6
D3-1	52.19	2.67	15.67	10.40	0.05	0.16	3.82	6.91	3.70	2.17	0.68	98.41	42.6
D3-2	52.27	2.59	15.85	10.33	0.00	0.23	3.72	6.86	3.73	2.09	0.49	98.15	42.1
D4-1	51.81	2.71	15.49	10.29	0.01	0.18	3.93	6.88	3.83	2.12	0.61	97.86	43.5
D4-2	52.00	2.61	15.83	10.34	0.02	0.19	3.80	6.74	3.61	2.18	0.73	98.06	42.6

*FeO** total Fe as FeO*, *Mg#* 100 $Mg^{2+}/(Mg^{2+}\ Fe^{2+})$, assuming $Fe_2O_3/FeO = 0.15$

fragments are also underrepresented in the medial-distal deposits because they occur mostly as blocks and lapilli in the proximal part of the tuff ring. In spite of these limitations, deep-derived accidental materials could be easily identified and precisely counted under microscope and on BSE images.

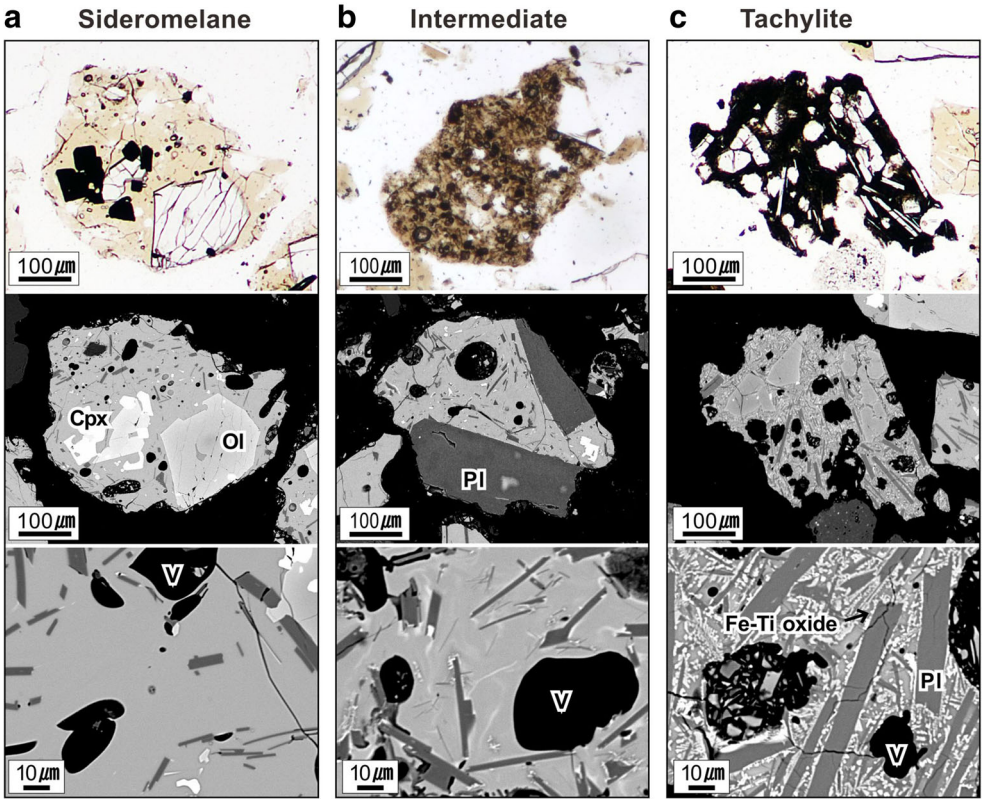

Fig. 6 Thin-section photomicrographs and BSE images of three types of juvenile grains. **a** Sideromelane grains have colorless to light yellow glassy groundmass under optical microscope (*top*) and pristine glass on the BSE images (*middle* and *bottom*) with scarce Fe-oxide microlites. **b** Intermediate grains have dark brown and translucent groundmass under optical microscope and intermediate amounts of Fe-oxide microlites. **c** Tachylite grains have opaque groundmass under optical microscope and densely populated microlites of Fe oxides that surround or coat the plagioclase laths on BSE images. *Cpx* clinopyroxene, *Ol* olivine, *Pl* plagioclase, *V* vesicle

Vertical componentry variations

The results of the componentry analysis are given in Table 2 and summarized in Fig. 8. The analysis shows that the content of the tachylite plus intermediate grains relative to sideromelane grains generally increases up-section with a dramatic decrease across the boundary between units B and C and a minor decrease across the boundary between units C and D (Fig. 8a). (The samples D3 and D4 were excluded from the analysis of the tachylite to sideromelane ratio and the ash-coated vs. uncoated tephra ratio

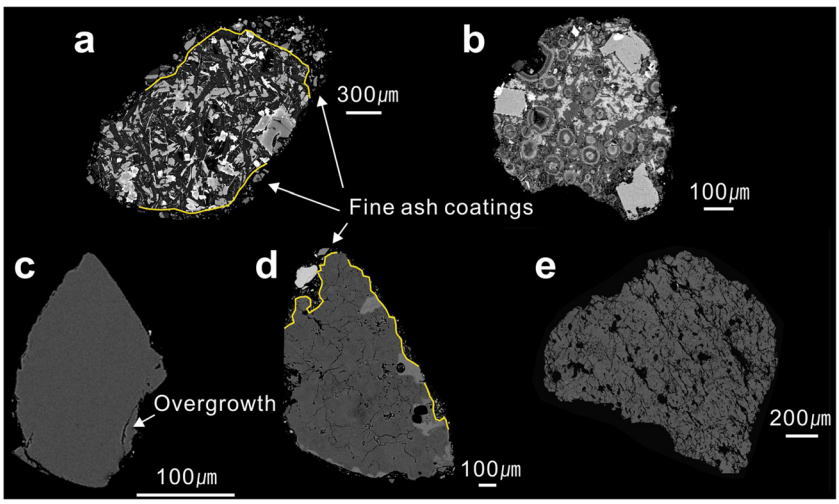

Fig. 7 BSE images of five types of accidental grains. **a** Crystalline basalt fragments from the underlying lavas contain abundant olivine and plagioclase phenocrysts in a microcrystalline groundmass rich in plagioclase laths. **b** Basaltic tuff fragments derived from the Seoguipo Formation consist of sideromelane or tachylite grains commonly with alteration or palagonitized rims along grain margins and vesicle walls. **c** Monocrystalline quartz grains derived mainly from the U Formation are generally angular and have quartz overgrowth along the grain margins, suggesting their origin from sedimentary rocks. **d** Polycrystalline quartz grains or quartzose rock fragments from the basement rocks show pervasive internal fractures and secondary pores. **e** An alkali feldspar grain with pervasive fractures and secondary pores also derived from the basement rocks. Note that some grains have partially preserved coatings of extremely fine ash along the grain margins

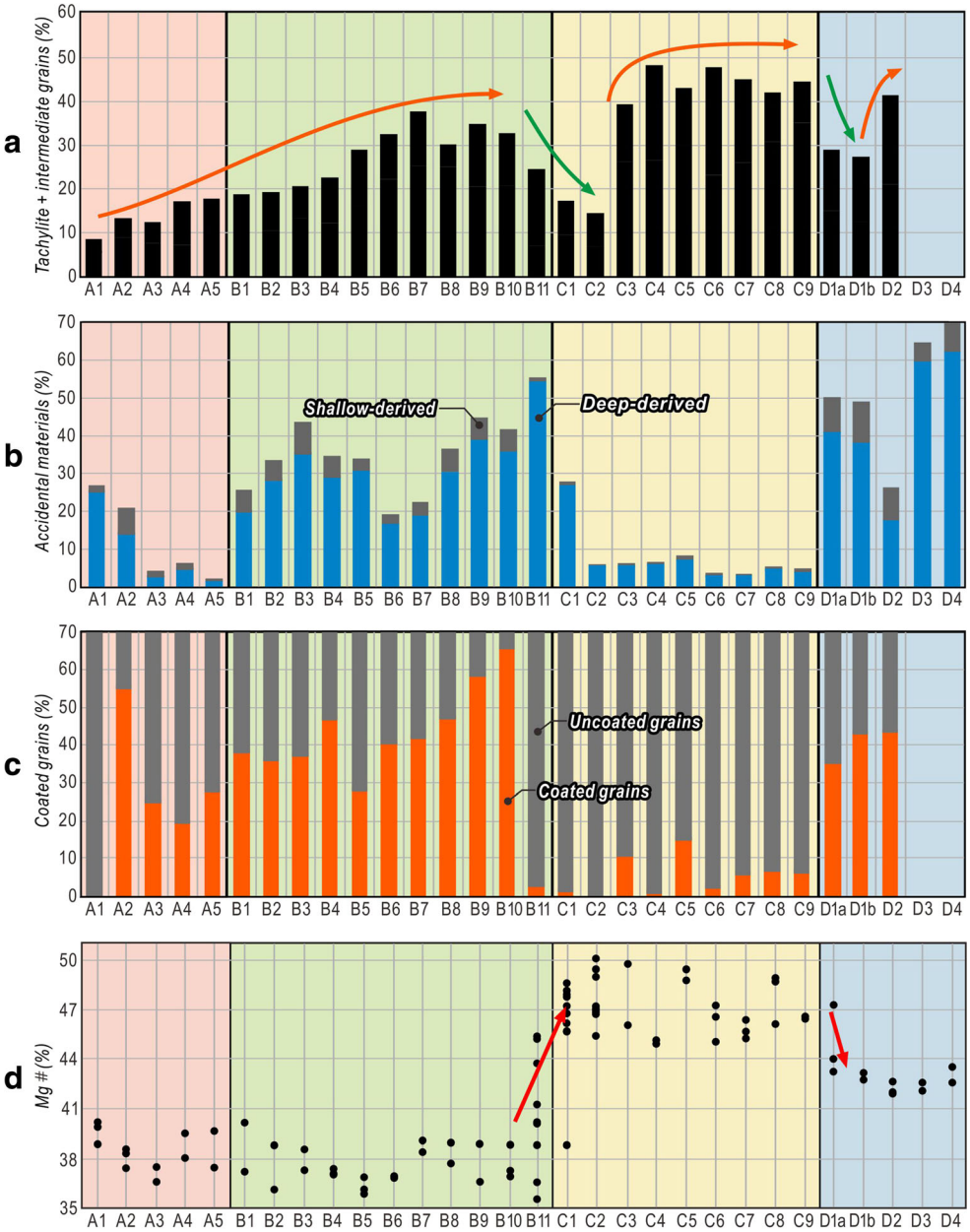

Fig. 8 Vertical variations in componentry in Songaksan tephra. **a** Variations of the proportion of tachylite and intermediate grains relative to the total of juvenile clasts, overall increasing up-section but with two drops across the boundaries between units B, C, and D. **b** Variations of the accidental componentry. The shallow-derived accidentals include crystalline lava and tuff fragments from the underlying lavas and the Seoguipo Formation. The deep-derived accidentals include monocrystalline to polycrystalline quartz grains and other accessory mineral grains derived from the U Formation and the basement rocks. **c** Variations of the proportions of ash-coated vs. uncoated tephra grains. Not a single ash-coated grain was found in samples A1 and C2. **d** Variations of the magnesium number of the glassy groundmass of sideromelane grains, suggesting three magma pulses. First pulse = samples A1 to B10, second pulse = samples B11 to C9, third pulse = D1 to D4

because of severe alteration of the juvenile grains in the upper part of unit D.)

The content of the deep-derived accidental grains shows marked variations between the tuff units (Fig. 8b). Units B and D contain 26.6 and 39.4% deep-derived accidentals (quartz and other accessory mineral grains) on average, respectively, and units A and C contain only 7.9 and 6.7% deep-derived accidentals on average, respectively (Table 2). Unit A is characterized by a progressive decrease of the accidental material content, whereas unit C is characterized by a uniformly low accidental material content (except in sample C1). It is also worth noting that the relative proportions of the shallow-derived vs. deep-derived accidental materials do not change significantly between units, except for unit C, which has extremely rare shallow-derived accidental materials.

We found during the componentry analysis that a large proportion of either juvenile or accidental grains are still coated by an extremely fine ash layer, a few micrometers in thickness (e.g., Fig. 7a, d), even after the treatment of the samples in an ultrasonic vibrator and the disintegration of ash lumps or aggregates with fingers before wet sieving. We thus decided to count the number of the ash-coated vs. uncoated grains in each sample and found that a large proportion of the grains in units A, B, and D are ash-coated whereas the grains of unit C are mostly uncoated (Figs. 8c and 9). We postulate that the distinctively black tuff color of unit C (Figs. 2c and 3) is mainly the result of

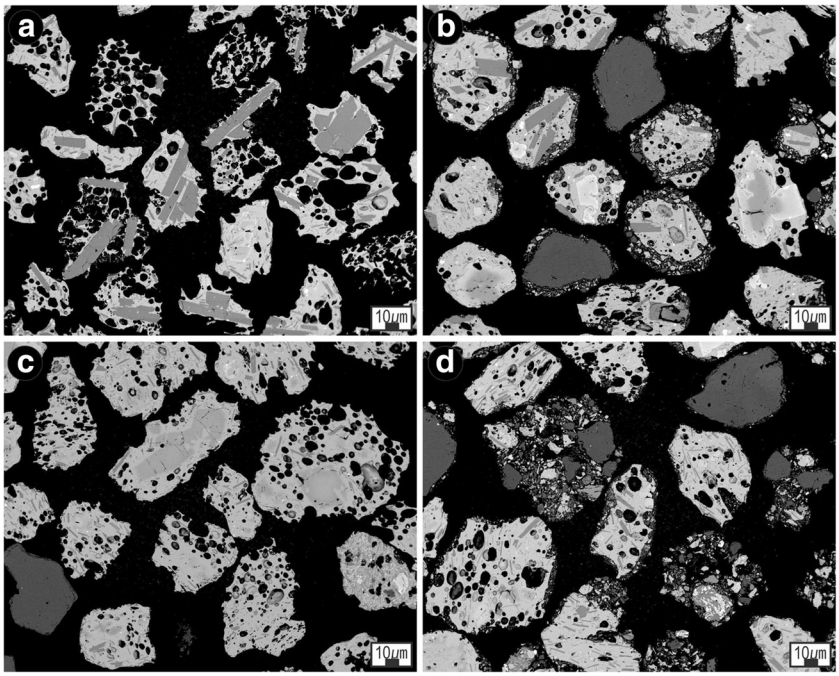

Fig. 9 BSE images of tephra grains showing marked contrasts in texture between tuff units. **a** Not a single tephra grain of sample A1 is ash-coated. Even the relics of coated ash are not found in the embayed vesicle walls along the grain margins. **b** Tephra grains of unit B (the image is from sample B4) are commonly coated by extremely fine ash whether they are juvenile or accidental. **c** Tephra grains of unit C (the image is from sample C2) are mostly uncoated by fine ash. **d** Tephra grains of unit D (the image is from sample D1b) show similar characteristics to those of unit B. The uncoated juvenile tephra grains of unit A1 (**a**) and unit C (**c**) preserve delicate grain margins in contrast to the coated tephra grains of unit B (**b**) and unit D (**d**), which are apparently better rounded

the lack of coated grains in addition to the rarity of accidental quartz grains. It was also interesting that the lowermost tephra bed of unit A (sample A1) and the topmost tephra bed of unit B (sample B11) consist entirely or mostly of uncoated grains in contrast to the other samples in the same tuff units.

Analysis of major element composition of the microlite-free glassy groundmass of sideromelane grains from each sample (Table 3) shows that the juvenile grains of units A and B and those of unit C have significantly different magnesium numbers (Mg#) and that the juvenile grains of unit D have Mg# intermediate between these units (Fig. 8d). The tephra grains from the topmost sample of unit B (sample B11) are also characterized by a range of Mg# intermediate between units A and B and unit C.

Subtle to significant differences in surface features of juvenile grains were found between the tuff units, although only qualitative observations were possible for these features because a significant portion of grains were coated by extremely fine ash. The observations show that some juvenile grains of unit A and most juvenile grains of unit C have sharp edges and relatively clean and curviplanar surfaces sparsely studded with extremely fine ash particles, less than a few micrometers in size (Fig. 10a, c). On the other hand, juvenile grains of units B and D have generally more abraded edges and moss-like surfaces due to a relatively thick cover of extremely fine ash particles, a few micrometers to a few tens of micrometers in size (Fig. 10b, d).

Interpretations

Variation of chemical composition

The significantly different Mg#s between the juvenile grains of units A and B and unit C and the moderate difference of Mg#s of unit D, which were also reported in a previous study (Ahn et al. 2015), suggest that there were at least three magma batches with different thermal histories during the eruption of the Songaksan tuff ring (Helz and Thornber 1987; Luhr 2001; Johnson et al. 2008; Del Gaudio et al. 2010; Johnson et al. 2010) (Fig. 8d). Brenna et al. (2011) inferred six magma batches for the entire volcanic sequence of Songaksan and four magma batches (one magma batch for each tuff unit) within the tuff ring. Sample B11 is of particular interest because of the wide range of Mg#s. The lower range of Mg#s in this sample (and the single low-Mg# data point in sample C1) is interpreted to represent existing juvenile clasts in the diatreme infill, that were ejected together with new particles having higher Mg#s. Those new particles in sample B11 have Mg#s intermediate between those of the first magma batch and those of the second batch, manifested in unit C. This means that magma from the second batch arrived in the feeder dike shortly before the eruption of unit C and mixed variably within the dike with the first batch of magma before fragmentation. By the time unit C was erupted, the feeder dike was entirely occupied by the second

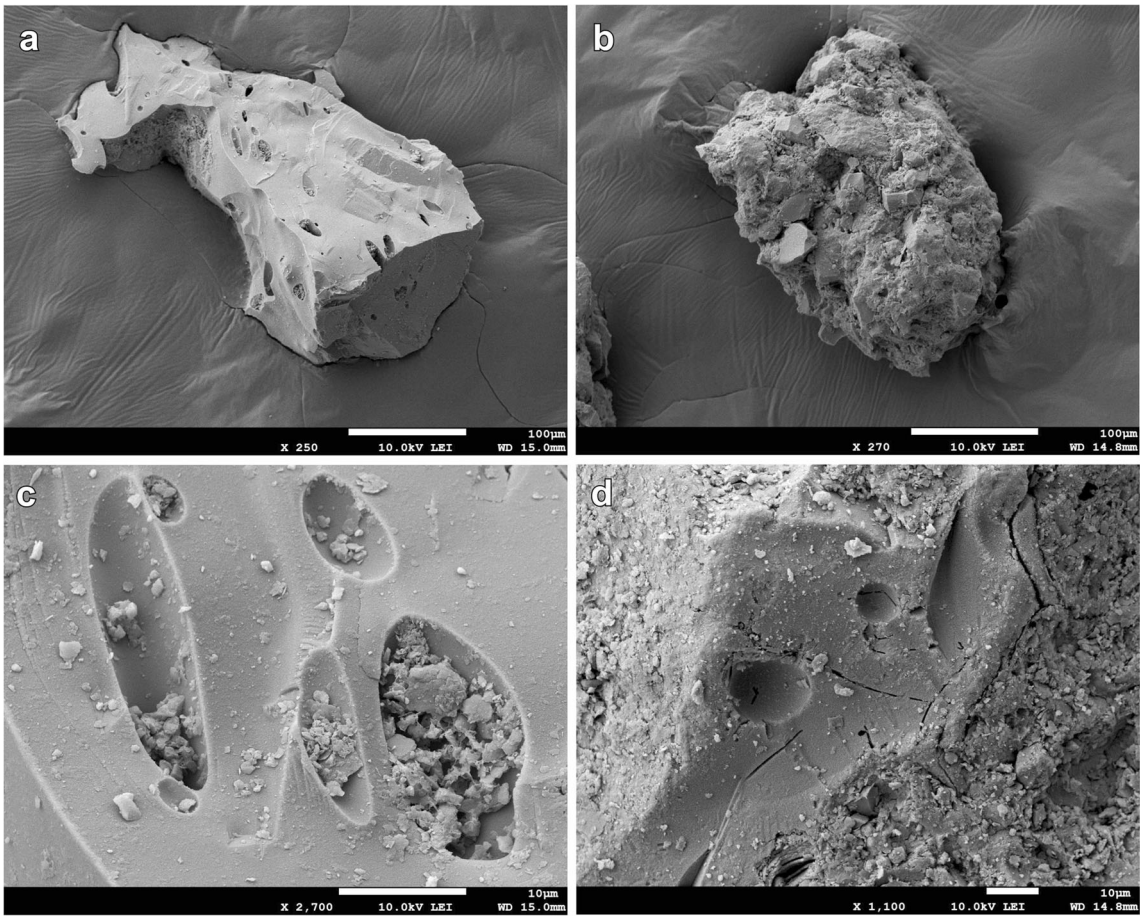

Fig. 10 Scanning electron microscope images of tephra grain morphology and surface features. **a** Blocky, angular, and uncoated juvenile grain of unit C. **b** Thickly ash-coated juvenile grain of unit B. **c** Close-up of the juvenile grain surface of unit C sparsely studded with extremely fine ash particles. **d** Close-up of the juvenile grain surface of unit B, looking dirty because of adhesion of abundant fine ash particles. The grain edges are not as sharp as those of unit C (c). Hydration or quench cracks are visible on the grain

magma batch. Another evidence for magma mixing during the eruption of unit B11 is provided by the common, but not unique, occurrence of olivine phenocrysts in the B11 tephra that have an Mg-poor and resorbed core surrounded by an Mg-rich and partially resorbed mantle or have an Mg-rich core surrounded by an Mg-poor mantle (Ahn et al. 2015).

We therefore interpret that the second magma batch rose through the same feeder dike where the residual magma from the previous eruptive phase still remained molten, thereby resulting in intimate mixing of the two magmas. This implies that the eruption of the earlier magma batch was immediately followed by the eruption of the second magma batch through the same feeder dike and vent without a break in eruption. We also make the same interpretation for the transition between units C and D. This interpretation is consistent with the field observations of the Songaksan tuff ring, which suggest a sequential but uninterrupted eruption of multiple magma batches through the same vent (Brenna et al. 2011). Songaksan is thus in contrast to some volcanoes, e.g., the Ilchulbong tuff cone, which experienced a quite long pause in eruption between the pulses of multiple magma batches, preserved as volcano-wide erosion and reworking of tephra, solidification of the residual magma within the feeder dike, and a shift in the location of the vent (Sohn et al. 2012).

Variation of accidental componentry

Accidental materials can be incorporated into the diatreme in a number of ways, including the explosion-induced destruction of the diatreme wall rocks near the explosion loci, gravity-induced collapse of the wall rocks and overlying tephra beds in the upper level of the diatreme, and scouring of wall rocks by debris jets and other gaseous to particulate flows (Barberi et al. 1989; Houghton and Nairn 1991; Ross and White 2006; White and Ross 2011; Delpit et al. 2014; Agustín-Flores et al. 2015). Variations of the types and amounts of the accidental materials can therefore provide indirect information on the changes in the dimension of the diatreme due to either lateral enlargement or downward excavation, although there are some complicating factors in that the ejecta from an explosion can comprise materials from different depths that were admixed by prior subsurface explosions (Graettinger et al. 2014; Graettinger et al. 2015;

Valentine et al. 2015). In the case of Songaksan, the amount of the deep-derived accidental materials are interpreted to reflect mainly disruption and excavation of the substrate below ca. 120-m depth, whereas the amount of the shallow-derived accidental materials are interpreted to reflect mainly lateral enlargement of the diatreme in the shallow level above ca. 120-m depth.

The componentry analysis (Fig. 8b) shows clearly that the diatreme growth occurred mainly during the eruption of the lower part of unit A and throughout the eruptions of units B and D. At other times, the diatreme appears to have remained quite stable, especially during the eruption of unit C. The relative rarity of the shallow-derived accidental materials in this unit and in the upper part of unit A also suggests that the growth of the diatreme in the upper level halted almost completely during deposition of these units. It is also worth noting that the proportions of the deep-derived vs. shallow-derived accidental materials do not show any temporal trend and that even the lowermost tuff bed of unit A contains as much deep-derived accidental materials as the tuff beds of the overlying units. We therefore interpret that the model for the growth of diatremes in response to deepening of phreatomagmatic explosion sites due to drawdown of the water table (Lorenz 1986) is not applicable to Songaksan because the inverted subsurface stratigraphy of the Songaksan area is not reflected in the vertical variations of the accidental componentry at all.

Variation of grain surface features

The proportion of coated grains shows important variations between units (Fig. 8c). We rule out the possibility of differential, post-eruptive, or post-depositional cementation of tuff for the origin of the ash coatings in some particular tuff units because there is no reason to suppose that there are, or were, significant differences in grain size characteristics, depositional setting, interstitial fluid properties, or other factors that can influence the degree of cementation between the tuff units. Above all, the tuff beds composed of ash-coated tephra are not cemented at all and as fragile as the tuff beds composed of uncoated tephra. The variations in the proportions of coated grains must therefore be primary.

Accretion of ash is normally thought to occur in eruption plumes and pyroclastic density currents (abbreviated as PDCs) as a result of electrostatic attraction and moist adhesion between particles (Gilbert and Lane 1994; Schumacher and Schmincke 1995; Brown et al. 2010; Brown et al. 2012). We first explored this idea, but rejected it because the coating or uncoating of tephra in different tuff beds could not be explained by the differences in the eruption and depositional processes. Above all, we could not find any relationship between the deposit features and the coating/uncoating of tephra. Our field observations, in addition to the previous field studies of Songaksan since the 1990s (Chough and Sohn 1990; Sohn et al. 2002; Yoon et al. 2016), indicate that the tuff beds that lack coated grains (samples A1, B11, and all samples of unit C) have the same suite of deposit structures as the other tuff beds such as megaripple bedforms, low-amplitude undulations, and planar to parallel bedding (e.g., Fig. 3). In particular, accretionary lapilli, adhesion ripples, and plastered tuffs, which are all indicative of the wetness of tephra, are found in all tuff units, suggesting that they originated from the same suite of depositional processes, i.e., moist pyroclastic surges and associated fallout, generated during explosive phreatomagmatic eruptions.

We therefore infer that the ash coatings formed in the diatreme rather than in the eruption plumes or PDCs. This inference is based on the reasoning that the diatreme is a place where interparticle collisions can occur much more frequently than in the eruption plumes or PDCs because of the high particle concentration of the diatreme fill. Probably, particle adhesion can occur promptly and efficiently in the diatreme if the conditions for particle adhesion are met. Possible controls of ash accretion processes in the diatreme include the degree of water saturation and the cohesiveness of the diatreme-filling debris, the nature of the coolant, whether it is clear water or muddy fluid, and the residence time and the degree of recycling and explosion-driven circulation of tephra within the diatreme.

Our hypothesis of ash accretion in the diatreme needs to be verified by further investigation of the microtextures of tephra in addition to an appraisal of the physical conditions and processes of ash accretion in the diatreme in comparison to those of ash accretion in eruption plumes and PDCs. We like to propose, however, that the diatreme can be another site of ash accretion in maar-diatreme volcanoes. Presently unresolvable question is why some tephra beds are completely or almost completely devoid of coated grains in spite of their apparent emplacement by moist pyroclastic surges and associated fallout, generated during explosive phreatomagmatic eruptions. The complete lack of ash-coated grains in some samples, not even the relics of ash coatings that might have been preserved inside the embayed vesicle walls along the grain margins (Fig. 9a, c) even after the procedures for sample preparation, suggests that the lack of ash coatings is not due to artificial effects but is primary. We interpret that uncoated ash was ejected from the diatreme by some eruptions, but there is still a chance of ash accretion of uncoated ash if the ash was transported through a moisture-rich eruption plume and PDC. We like to leave this question unanswered for a future research of ash accretion processes in phreatomagmatic volcanoes.

Variation of tachylite to sideromelane ratios

Clear and pale-colored basaltic glass named sideromelane is produced by rapid chilling of basaltic magma, whereas less rapid chilling of the magma results in tachylite, which is deep-brown to opaque in thin sections due to incipient growth of opaque minerals, mainly magnetite (Peacock and Fuller

1928; Heiken and Wohletz 1985). One plausible hypothesis that can explain the variations of the cooling rate of magma and the relative abundance of sideromelane to tachylite in basaltic volcanoes is the change of magma flux and the evolution of the velocity gradient of ascending magma within a volcanic conduit (Taddeucci et al. 2004; Sable et al. 2006). According to this hypothesis, the gradual increase of the tachylite in the tephra layers from the first magma pulse (sample A1 to B10) as well as the rather abrupt increases of the tachylite in the tephra layers from the second (sample B11 to C9) and the third (sample D1a to D2) magma pulses (Fig. 8a) indicate that the magma that arrived at the diatreme later in each pulse experienced a longer residence time in the upper conduit because of decreasing ascent velocity of magma during the pulses. Alternatively, increasing proportions of tephra might have been produced by explosive disruption of previously intruded blobs of magma which underwent longer periods of cooling within the diatreme during each magma pulse, thereby resulting in the gradual to abrupt increases in the proportions of tachylitic grains relative to sideromelane grains. The contrasts in vesicle shapes between the sideromelane, which generally have oval vesicles, and the tachylitic grains, which generally have irregular vesicles (Fig. 6), suggest that the tephra from the same ejecta beds can comprise a variety of grains that had different residence times in the diatreme and were subjected to different degrees of cooling in the diatreme.

The sideromelane grains are interpreted to have formed by fragmentation of the relatively phenocryst-poor and microlite-poor and hotter zone of the ascending magma, as indicated by the relatively rare and small plagioclase laths (Fig. 6a), or by instantaneous molten fuel-coolant interaction of a newly arrived and uncooled magma with the diatreme fill as soon as the magma intrudes into the diatreme. On the other hand, the tachylite grains are interpreted to have formed by fragmentation of the microlite-rich and cooler magma in the peripheral zone of the ascending magma or by fragmentation of previously intruded blobs of magma which underwent longer periods of cooling in the diatreme and thereby have irregular, "contracted and shrunk" vesicles. Explosive disruption of materials produced by transient magmatic activity is another possibility to produce tachylite grains, although we have not found any evidence for such magmatic activity (e.g., scoria deposits) even in the most proximal part of the tuff ring.

The overall increase of the tachylite content throughout the tuff sequence (Fig. 8a) and the transition of the eruption style to the Strombolian and Hawaiian eruptions, which resulted in the nested scoria cones and ponded lava inside the crater of the tuff ring (Fig. 1c), suggest a gradual decrease in magma flux or eruption rate and the formation of degassed marginal magma along the conduit walls, which eventually sealed off water access to the magma after solidification (Taddeucci et al. 2004; Sable et al. 2006). Alternatively, an increase in magma flux might have led to the transition to magmatic eruption style because magma-water interaction can be no longer effective when the magma flux is very high. In this case, the increase of tachylite can be explained by an increase in the proportion of juvenile materials that were explosively disrupted from previously intruded and cooler blobs of magma in the diatreme.

Diatreme dimension

The minimum diatreme dimension of Songaksan was estimated by calculating the volume of the entrained materials from the substrate. First, the volume of the proximal-to-medial tuff ring was calculated by taking into account the height and area of individual topographic contours above 10-m altitude with an assumption that the contours of the tuff ring before erosion were circular and concentric. The estimate of the proximal-to-medial tuff ring is 0.061 km^3. The volume of the distal tuff ring outside the 10-m contour was calculated as 0.033 km^3 following the exponential model of Pyle (1989). The total volume of the tuff ring is therefore estimated to be ca. 0.1 km^3. The actual volume of the Songaksan tephra is assumed to have been at least twice the volume of the tuff ring if we take into account the fine ash lost by fractionation processes during transport, which can be as much as 50% of the erupted volume of a magma (Walker 1972; Sparks and Walker 1977), and those tephra that failed to escape the diatreme, which can have a volume comparable to that of the volcanic edifice on the surface (White and Ross 2011).

The average contents of deep-derived accidental materials in individual tuff units are 9.5% (unit A), 30.7% (unit B), 7.5% (unit C), and 43.7% (unit D) (Table 2). The average content of deep-derived accidental materials within the whole tuff ring is estimated to be ca. 22% when considering the relative thicknesses of the individual tuff units, which comprise ca. 20% (units A and D) and 30% (units B and C) of the tuff ring (see Fig. 2a for visual estimation). Although the componentry data were obtained only from 0 to 4 Φ fractions of tephra, qualitative observations of the coarser and finer fractions suggest that the deep-derived accidental materials are fairly evenly distributed in these size fractions too, as in the 0 to 4 Φ fractions. We thus estimate that ca. 22% of the total erupted tephra (0.2 km^3), i.e., ca. 0.04 km^3, were excavated from the U Formation and the quartzose basement rocks. If the excavation was confined to a cone, the height of the cone, having a volume of 0.04 km^3 and a radius of 0.3 km at the top, is calculated to be ca. 460 m. The radius of the cone at the top was determined by measuring the diameter of the crater rim of the tuff ring on the map, with an assumption that the arcuate topographic contours of the remaining tuff ring were originally circular before erosion, and by measuring the dip of the inner crater wall of the tuff ring in the field. The diatreme wall above the U Formation was assumed to be vertical. The minimum depth of excavation, including the thicknesses of the lavas and the Seoguipo

Formation (ca. 120 m), is therefore estimated to be about 580 m (Fig. 11). The calculated dimension of the cone provides the minimum estimate of the diatreme size and depth because only part of the disrupted material in the subsurface diatreme is eventually ejected from the diatreme and deposited in tephra rings (Ross et al. 2013; Taddeucci et al. 2013; Graettinger et al. 2014; Graettinger et al. 2015).

According to the reconstruction of the diatreme, ca. 0.03 km^3 of accidental materials are supposed to have been derived from the lavas and the Seoguipo Formation together with ca. 0.04 km^3 of deep-derived accidental materials. The total amount of the shallow-derived accidental materials estimated from the componentry analysis is much smaller than the calculated value, suggesting that the majority of the accidental materials from the shallow substrate were deposited in the proximal tuff ring or retained within the subsurface diatreme probably because of their large clast sizes. The total bulk volume of juvenile tephra is estimated to be ca. 0.13 km^3 (0.20 minus 0.07 km^3), and the volume of magma before vesiculation to be ca. 0.08 km^3 based on 8% calculated vesicularity of juvenile clasts and 35% measured porosity of the deposit (Sohn 2015). If the tuff ring erupted over a period of a month, which is the minimum estimate of the eruption duration based on the sedimentary records of tides during the eruption of Songaksan (Yoon et al. 2016), the magma flux might have been as high as 33 m^3/s, which is within the typical range of magma fluxes of monogenetic volcanoes (Pioli et al. 2009). Phreatomagmatic explosions might have been repeated with an interval of a few seconds to a few minutes if the individual explosions involved 10^2–10^4 m^3 of magma (Zimanowski and Buttner 2002).

Diatreme evolution

Substrate condition

Volcanic, volcaniclastic, and sedimentary rocks of Jeju Island are generally characterized by high permeability and high groundwater storage capacity and comprise the main aquifers of the island (Hahn et al. 1997; Kim et al. 2003; Won et al. 2005; Koh et al. 2006; Won et al. 2006; Mair et al. 2013). The groundwater table in the Songaksan area was probably very close to sea level by the time of eruption of the volcano as it is at present. The lavas beneath Songaksan have high-permeability groundwater storage space because of numerous joints and cavities (e.g., lava tubes) in the lavas and intervening clinker and scoria layers (Koh 1997; Won et al. 2006). The Seoguipo Formation is variably permeable and porous because the formation comprises both poorly sorted and indurated volcaniclastic rocks that can act as

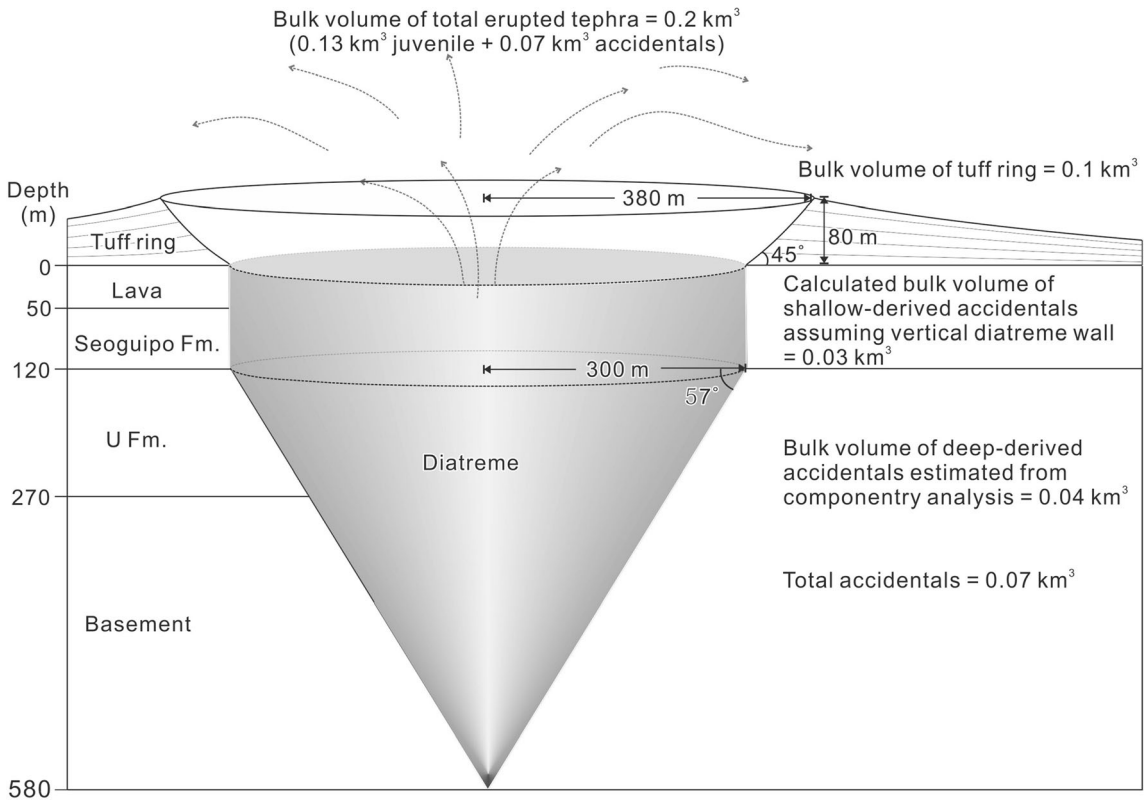

Fig. 11 Reconstruction of the dimension and geometry of the Songaksan diatreme with an assumption that the accidental materials were derived only from the inverted cone. The dip of the diatreme wall is estimated to be 57° beneath the Seoguipo Formation. The diatreme wall above the U Formation was assumed to be vertical.

aquicludes or aquitards and well sorted and unconsolidated volcaniclastic and non-volcaniclastic deposits that can act as aquifers. The U Formation is the most porous and permeable because its main constituent is well sorted and unconsolidated sand. The quartzose basement rocks are also inferred to be porous and permeable because of the development of pervasive fractures and secondary pores (Figs. 4c and 7d). These substrate conditions beneath Songaksan appear to have allowed the ascending magma to begin explosive magma-water interactions at any level in the subsurface because the subsurface strata, which were probably all water-saturated, occur at depths where water pressure is well below the critical pressure of water (Zimanowski et al. 1997).

Initial cratering

The lowermost tephra beds that were sampled at the medial-distal location (Fig. 2a) may not represent the products of the earliest eruptions. It is highly probable that the earliest eruptions ejected an abundance of coarse-grained lava and volcaniclastic rock fragments from the relatively hard, shallow-level substrate, less than ca. 120 m in depth (Fig. 12a). It is also likely that there were pre-eruption explosions in the subsurface, which disturbed the subsurface strata and caused vertical mixing of the disturbed materials but failed to eject any material to the surface. The deposit evidence for the earliest eruptions is probably hidden in the unexposed lowermost part

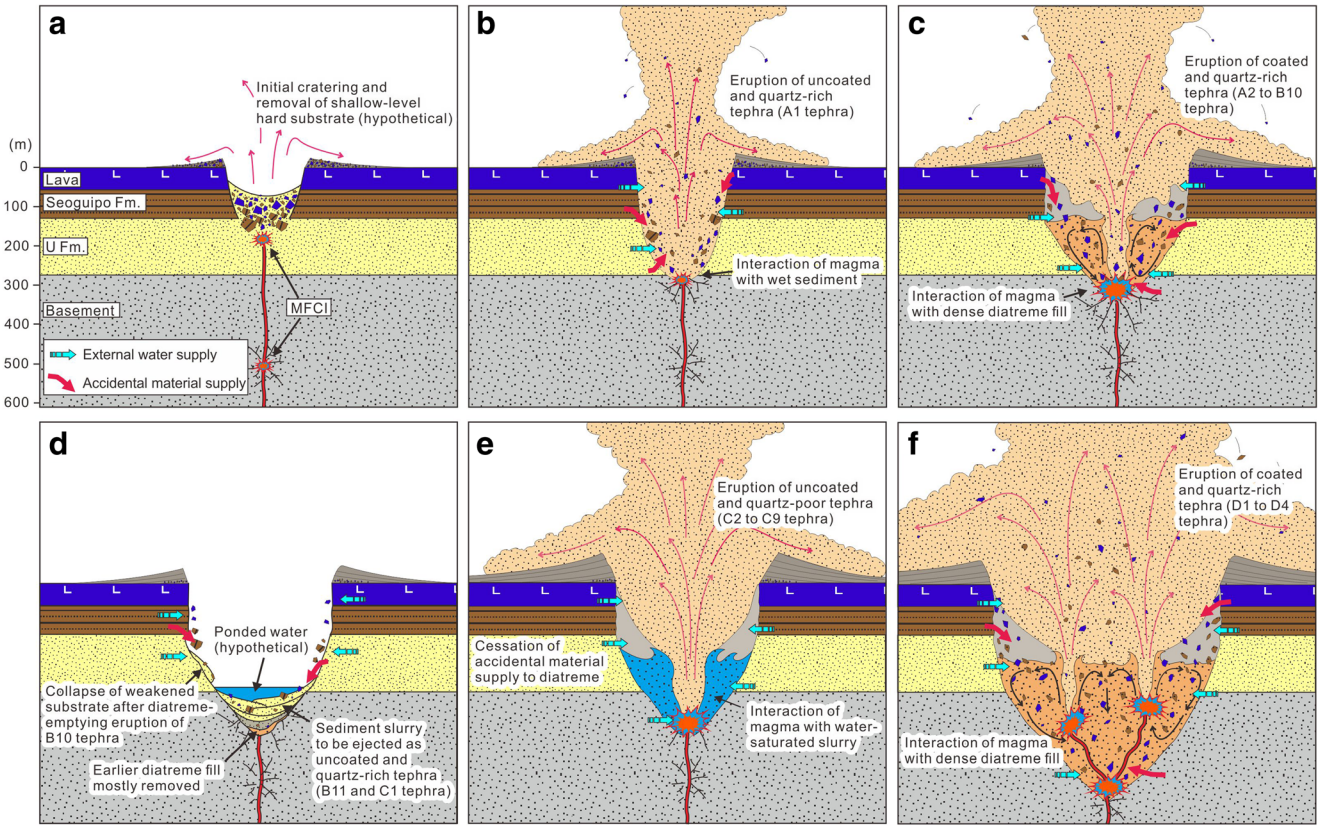

Fig. 12 Illustration of the evolution of Songaksan diatreme. **a**crystallineThe relatively hard shallow-level substrate is presumed to have been removed by an initial cratering eruption, probably exposing the sedimentary substrate before eruption of the medial-to-distal tephra beds. **b** The basal tephra layer at the medial-to-distal location of the tuff ring (sample A1) was produced by an explosion within or beneath an unconsolidated subsurface sedimentary formation, ejecting abundant quartzose materials. The tephra grains are unabraded and uncoated because they have not yet experienced recycling and pre-eruption mixing in the diatreme. **c** The majority of the later eruptions ejected abraded and fine ash-coated tephra, suggesting phreatomagmatic explosions in the presence of wet and cohesive diatreme fill. **d** The diatreme was almost completely emptied by the time of eruption of B10 tephra, leaving a deep crater. The removal of lateral support by the diatreme fill led to collapse of the disrupted and fragile substrate around the diatreme margins, resulting in a quartzose diatreme fill above the residual earlier diatreme fill. The quartzose diatreme fill was removed again by the following eruptions of B11 and C1 tephra. **e** By the time of onset of the eruption of unit C, the diatreme was stabilized, and the supply of accidental materials to the diatreme stopped almost completely. Magma flux into the diatreme might also have been reduced. Because of the reduction in the supply of solid materials, the diatreme fill became supersaturated with water, thereby inhibiting fine particle adhesion. The unit C eruption thus ejected mostly uncoated and unabraded tephra grains with rare accidental materials. **f** Return to "normal" diatreme condition of unit D, under which magma interacted with dense diatreme fill that was undersaturated with water. External water supply to the diatreme was unexhausted throughout the eruption of the tuff ring because of the high permeability and groundwater storage capacity of the substrate. The diatreme was depicted as an inverted cone, ignoring possible irregularity of the subsurface structure due to disruption of the substrate surrounding the diatreme. *MFCI* molten fuel-coolant interaction

of the proximal tuff ring or has subsided into the diatreme as a result of later diatreme enlargement if the earliest ejecta were dispersed only a few hundred meters away from the initial eruptive center. Some large chunks of lavas and volcaniclastic rocks torn from the shallow substrate might never have been ejected to the surface but instead have sunken into the sediment of the U Formation (Fig. 12a), which probably had lost its strength because of explosion-induced disturbance of the substrate.

Eruption of A1 tephra

After the initial cratering of Songaksan that removed the majority of the shallow-level substrate (Fig. 12a), the lowermost tephra beds at the medial-distal location (samples A1 and A2) were formed (Fig. 12b, c). These beds contain much more deep-derived accidental materials than shallow-derived materials (Fig. 8b). For sample A1, the explosions were probably caused by molten fuel-coolant interaction of magma with the wet sediment of the U Formation and vented abundant quartzose materials to the atmosphere (Fig. 12b). The U Formation might have been exposed to the atmosphere at that stage because of the removal of the overlying rocks by earlier cratering eruptions. The total absence of ash-coated grains in sample A1 (Figs. 8c and 9a), not even the relics of ash coatings that might have been preserved inside the embayed vesicle walls along the grain margins, suggests that the accidental materials were instantaneously ejected into the atmosphere together with freshly fragmented juvenile materials, without prolonged pre-eruption mixing in the subsurface, probably because of the poor development of a diatreme structure in the early stage of the Songaksan eruption, in which grain adhesion could occur as a result of explosion-driven mixing of accidental and juvenile materials.

Eruption of A2 tephra

The abrupt increase in the amount of ash-coated grains in sample A2 (Fig. 8c), directly above the tephra bed of sample A1, suggests that a significant portion of the tephra produced by the earlier eruptions failed to escape the diatreme and participated immediately in the explosion-driven mixing of debris in the diatreme. The tephra thus appears to have been coated by the fine materials of the diatreme fill, which was probably wet and sticky, until the tephra was ejected by the next eruption together with freshly fragmented and uncoated tephra grains (Fig. 12c). The abrupt change in the character of tephra grains between samples A1 and A2 suggests either that the process of ash coating was very prompt in the diatreme or that there were smaller explosions between deposition of A1 and A2 tephra beds, which were confined to the crater but led to explosion-driven mixing of the diatreme-filling debris.

Eruption of A3 to B10 tephra

The rarity of accidental materials in samples A3 to A5 suggests that the supply of accidental materials to the actively circulating zone (referred to as "active zone" hereafter) of the diatreme was greatly reduced, probably because of the temporary pause of diatreme growth until the onset of eruption of unit B. The sudden increase in the contents of both shallow-derived and deep-derived accidental materials in unit B (Fig. 8b) suggests that an abundance of accidental materials began to be supplied to the active zone of the diatreme from various levels of the substrate, probably involving gravity-induced collapse of the wall rocks in the upper level of the diatreme and explosive excavation and upward mixing of accidental materials from the deeper level of the diatreme. The diatreme is therefore inferred to have grown significantly both vertically and laterally during the eruption of unit B at the expense of the accidental materials that were removed from the substrate. The abundance of ash-coated grains in this unit also suggests that the explosions continued to be generated by the interaction of magma with wet and cohesive diatreme-filling debris (Fig. 12c).

Eruption of B11 and C1 tephra

The diatreme fill, which probably comprised abundant ash-coated tephra, is interpreted to have fluctuated in its volume during the eruption of unit B but have been eventually removed by the time of eruption of B10 tephra because the overlying tephra beds from the second magma batch (samples B11 to C9) are almost devoid of ash-coated grains (Fig. 8c) and of the juvenile grains from the first magma batch (samples A1 to B10) that have low Mg# (Fig. 8d). So, there would have been a deep empty crater after the eruption of sample B10, which is the last to have been solely produced by the first (low Mg#) magma batch (Fig. 12d). The second, higher Mg#, magma batch started to arrive in the feeder dike in time to form sample B11 (Fig. 8d). It mixed with the existing magma in the dike to produce intermediate Mg#s during B11 time, but the dike was entirely occupied by the second magma batch by C1 time, and this new magma continued to erupt during formation of unit C.

One alternative to the deep empty crater idea is that the earlier diatreme fill might have been left in the diatreme but was unused throughout the eruption of the second magma batch (during formation of samples B11 and later) because of very shallow explosions of the second magma above the earlier diatreme fill. This possibility, however, raises the following questions:

1. Why did the second magma avoid explosive interaction with the earlier diatreme fill left in the diatreme?

2. What could possibly act as the "coolant" for the phreatomagmatic explosions of the second magma above the earlier diatreme fill, if the explosions occurred sufficiently shallowly not to entrain any coated tephra from the earlier diatreme fill?

In the case of the B11 tephra, which contains abundant accidental quartz grains (>50%) but few coated grains (Fig. 8), it is hardly conceivable for an explosion to eject only freshly fragmented or freshly entrained and uncoated juvenile/accidental materials after entraining such an abundance of quartzose materials from somewhere in the diatreme, if the diatreme was filled with ash-coated tephra from earlier eruptions. It is neither likely that such an abundance of quartzose materials could be entrained from the deeper level of the substrate, transported to the upper level of the diatreme after passing through the diatreme-filling ash-coated debris by explosion-driven upward mixing, but neither be admixed with the debris nor be ash-coated at all, and then be ejected to the surface by the final shallow explosion above the earlier diatreme fill where it is dubious whether there was any material that could act as a coolant for phreatomagmatic explosions. We thus prefer a simple scenario of diatreme emptying by the time of the eruption of B10 tephra to a rather complex scenario of shallow explosions above an earlier diatreme fill throughout the eruption of the second magma batch.

The earliest eruption of the second magma batch, represented by sample B11, ejected abundant freshly entrained and uncoated accidental materials together with uncoated juvenile grains (Fig. 8b, c). This suggests that the disrupted and fragile substrate around the diatreme margins collapsed promptly into the diatreme after the eruption of the B10 tephra because of the removal of lateral support by the diatreme fill (Fig. 12d). The collapsed material, which was composed mainly of quartzose sand, probably formed a wet sediment slurry at the bottom of the diatreme that could act as a coolant for the phreatomagmatic eruption of the B11 tephra (Fig. 12d). The sediment slurry is interpreted to have been instantaneously ejected by the eruption of the tephra, not having a chance to be ash-coated in the diatreme. The remaining sediment slurry after the eruption of the B11 tephra appears to have been mostly consumed by the next eruption that formed the C1 tephra because of the overall lack of quartzose accidental materials above this tephra bed (Fig. 8c).

Eruption of C2 to C9 tephra

Throughout the eruption of samples C2 to C9, which are especially quartz-poor (Fig. 8b), the supply of accidental materials to the active zone of the diatreme appears to have been greatly reduced or almost cut off because of temporary stabilization of the diatreme structure (Fig. 12e). We envisage that the diatreme could be stabilized temporarily during the eruption of these tephra beds because of the removal of the disrupted or remolded and fragile substrate around the diatreme margins by previous eruptions. The diatreme fill is inferred to have been regenerated from the materials from the second magma batch and composed almost entirely of juvenile materials with high Mg#.

The rarity of ash-coated grains throughout the unit, which probably resulted in the particularly black tuff color of unit C (Figs. 2 and 3), suggests that some special condition was developed inside the diatreme, which inhibited the production of ash-coated tephra grains. Probably, the diatreme was filled with a water-saturated slurry, in which diatreme-filling tephra grains could be almost "suspended" in water (Fig. 12e). In such a wet slurry, fine particles would not adhere to larger ones because of the lack of surface tension effects of wet tephra grains (Schumacher and Schmincke 1995).

It is inferred from the componentry data that the supply of accidental materials to the diatreme was greatly reduced because of temporary stabilization of the diatreme during the eruption of unit C. The supply of juvenile materials might also have been reduced because of the reduction in magma flux to the diatreme. The relatively higher content of tachylitic grains in unit C (Fig. 8a) can possibly be the result of the reduced magma flux. The reduction in the supply of either or both of accidental and juvenile materials relative to the supply of external water to the diatreme probably resulted in water saturation of the diatreme fill. The external water consumed and lost by phreatomagmatic explosions could probably be promptly resupplied to the diatreme through the generally permeable substrate, maintaining the diatreme fill in a water-saturated condition throughout the eruption of unit C. The generally sharp and unabraded edges of juvenile grains in unit C (Fig. 9c and 10a, c) can be explained by the supersaturated nature of the diatreme-filling slurry because abrasion of grains would be greatly diminished if they are suspended in water, rather than making rubbing motions between contacting grains within a dense, undersaturated diatreme fill.

An alternative hypothesis for the tachylite-rich, accidental-poor, nature of unit C is that there might have been a brief period of magmatic activity that produced deposits confined to the crater. Then, this material was affected by shallow explosions which ejected it. We reject this alternative hypothesis for the following reasons:

1. Our ongoing study of Songaksan to measure the paleomagnetic signatures of temperatures that were experienced by lithic clasts from their eruption to final emplacement (Ahn and Sohn, unpublished data) suggests that unit C resulted from "colder" eruptions than the other units, near or below the boiling temperature of water, negating the possibility of magmatic eruption of unit C.
2. The tephra grain morphology and vesicularity (Figs. 6, 9, and 10) also negate the possibility of the recycling or

reuse of juvenile materials produced by a preceding magmatic activity.

3. It is also worth noting that the tephra of unit C has generally much higher contents of extremely fine ash finer than 4 Φ (Fig. 5), also suggesting fine fragmentation of magma by phreatomagmatic explosions.

Eruption of unit D

After the eruption of unit C, the diatreme condition was restored to the previous state, filled again with water-undersaturated debris (Fig. 12f). Probably, there was an abrupt increase in the supply of accidental materials from the diatreme margins at various levels, as indicated by the abrupt increase in the contents of both shallow-derived and deep-derived accidental materials in unit D (Fig. 8b). Therefore, an eruption similar to that of unit B could resume, ejecting an abundance of ash-coated tephra, containing abundant accidental materials. The diatreme is also interpreted to have been further enlarged during the eruption of unit D (Fig. 12d).

The transition from unit C to unit D occurred when the third magma batch [the fourth magma batch of Brenna et al. (2011)] arrived at the diatreme. The near absence of juvenile tephra from the second magma batch in unit D (Fig. 8d) suggests that the diatreme fill was once again renewed with new magmatic materials as the eruption of unit D commenced. We therefore postulate that the diatreme fill can be repetitively renewed during the eruption of a maar-diatreme volcano, possibly with an interval of almost complete diatreme emptying. The apparent correlation between the arrival of new magma batches and the transition between the tuff units with different componentry also casts an intriguing question of whether the correlation is coincidental or is the result of a causal link between the pulses of magma from the mantle and the diatreme processes near the surface of the Earth.

Post-tuff ring eruptions

The eruption changed eventually to a Strombolian/Hawaiian eruption, producing the nested scoria cone and ponded lava in the tuff ring. The scoria and lava were formed by two other magma batches that are distinct from the tuff ring, attesting to considerable chemical variations of magma during the eruption of Songaksan (Brenna et al. 2011). The transition was probably associated with a decrease in magma flux or eruption rate and the sealing off of water to the ascending magma because of solidification of marginal magma along the conduit walls (Taddeucci et al. 2004; Sable et al. 2006). Otherwise, magma flux might have increased to result in the transition to magmatic eruption because magma-water interaction can be no longer effective when the magma flux is very high.

Conclusions

The Songaksan tuff ring, Jeju Island, Korea, was produced by a single continuous eruption of multiple magma batches in an intertidal region ca. 3.7 ka BP. The whole tuff sequence consists of thin-bedded and well-bedded tuffs with abundant undulatory bedforms and accretionary lapilli in the middle-to-distal part, suggesting emplacement by dilute and moist pyroclastic surges and associated fallout. The high permeability and groundwater storage capacity of the substrate beneath Songaksan probably facilitated sustained phreatomagmatic activity throughout the eruption of the tuff ring.

In spite of the apparently identical deposit facies, the tuff sequence can be divided into four distinct units (A to D) with different colors and componentry. The basal tephra bed of unit A comprises only freshly fragmented juvenile grains and freshly entrained and mainly deep-derived (>120 m) accidental grains, suggesting instantaneous ejection of materials that had not yet experienced recycling and pre-eruption mixing in the diatreme. It is presumed that there was a prior cratering phase which removed the relatively hard shallow-level (<120 m deep) substrate and exposed the soft sedimentary substrate to the atmosphere before eruption of the basal tephra bed. Significant proportions of the juvenile and accidental grains in the overlying tephra beds of unit A, the majority of unit B, and unit D have abraded edges and thick ash coatings, suggesting that the ejecta from the later eruptions comprised an abundance of "recycled" or "premixed" tephra grains from earlier eruptions or earlier subsurface explosions.

Unit C is unique in that the tephra contains rare accidental materials, few ash-coated grains, and few or no sideromelane grains with low Mg# from the earlier magma batch. The componentry of unit C suggests that the earlier diatreme fill was almost completely removed and then regenerated with new materials from the second magma batch. There can be different explanations for the near absence of the earlier erupted tephra grains in the later-erupted ejecta beds with the explosions occurring in the presence of the earlier diatreme fill. But we prefer the possibility of simple diatreme emptying by a powerful explosion, following the principle of Occam's razor. The lack of ash-coated grains in unit C is attributed to water saturation of the diatreme fill, in which fine-particle adhesion was inhibited. Such a wet eruptive condition of unit C was possible because of the reduction of the supply of accidental materials to the diatreme and, possibly, the reduction in magma flux into the diatreme. The high permeability and groundwater storage capacity of the substrate must have been a prerequisite for such an eruption.

There have been significant advances in understanding diatreme processes because of recent studies of subsurface explosions and their products and the efforts to connect between theories and experimental and field observations (Carrasco-Núñez et al. 2007; Ross et al. 2008; Sottili et al.

2009; Taddeucci et al. 2010; Gernon et al. 2013; Ross et al. 2013; Taddeucci et al. 2013; Graettinger et al. 2014; Valentine et al. 2014; Valentine et al. 2015 among others). But the case study at Songaksan shows that there is still much room for further investigation of the details of the diatreme processes from the tephra rings. For example, this study shows that the diatreme fill can be completely removed and then regenerated during the eruption of a tuff ring, possibly in concert with the pulses of magma, thereby resulting in significant changes in the proportions of juvenile vs. accidental materials and fresh vs. recycled materials. This study also casts a presently unresolved question of how the eruption columns and pyroclastic density currents could remain virtually unchanged throughout the eruption of the tuff ring, resulting in the grossly similar deposit facies throughout the whole tuff sequence, in spite of the inferred variations of the diatreme conditions and processes.

Acknowledgments This work was supported by the Basic Science Research Program (NRF-2014R1A2A1A11053516) through the National Research Foundation of Korea funded by the Ministry of Education. We thank G. Valentine, an anonymous reviewer, and Associate Editor P.-S. Ross for their thorough and constructive comments on the manuscript.

References

Agustín-Flores J, Németh K, Cronin SJ, Lindsay JM, Kereszturi G (2015) Shallow-seated explosions in the construction of the Motukorea tuff ring (Auckland, New Zealand): evidence from lithic and sedimentary characteristics. J Volcanol Geotherm Res 304:272–286

Ahn US, Sohn YK, Yoon WS, Ryu CK, Jeong JO, Kang CW (2015) Geochemical fingerprinting of basaltic glass in tephra deposits underlying the human footprints-bearing strata in Jeju Island, Korea: provenance of tephra and age of the human footprints. J Geol Soc Korea 51:105–126 (in Korean with English abstract)

Auer A, Martin U, Németh K (2007) The Fekete-hegy (Balaton Highland Hungary) "soft-substrate" and "hard-substrate" maar volcanoes in an aligned volcanic complex—implications for vent geometry, subsurface stratigraphy and the palaeoenvironmental setting. J Volcanol Geotherm Res 159:225–245

Barberi F, Cioni R, Rosi M, Santacroce R, Sbrana A, Vecci R (1989) Magmatic and phreatomagmatic phases in explosive eruptions of Vesuvius as deduced by grain-size and component analysis of the pyroclastic deposits. J Volcanol Geotherm Res 38:287–307

Brenna M, Cronin SJ, Nemeth K, Smith IEM, Sohn YK (2011) The influence of magma plumbing complexity on monogenetic eruptions, Jeju Island, Korea. Terra Nov. 23:70–75

Brenna M, Cronin SJ, Smith IEM, Sohn YK, Maas R (2012) Spatio-temporal evolution of a dispersed magmatic system and its implications for volcano growth, Jeju Island Volcanic Field, Korea. Lithos 148:337–352

Brenna M, Cronin SJ, Kereszturi G, Sohn YK, Smith IEM, Wijbrans J (2015) Intraplate volcanism influenced by distal subduction tectonics at Jeju Island, Republic of Korea. Bull Volcanol 77:7

Broch E, Franklin JA (1972) The point-load strength test. Int J Rock Mechanics and Mining Sciences and Geomechanics 9:669–676

Brown ET (1981) Rock characterization testing and monitoring. ISRM suggested methods. International Society for Rock Mechanics, Salzburg, p 212

Brown RJ, Branney MJ, Maher C, Dávila-Harris P (2010) Origin of accretionary lapilli within ground-hugging density currents: evidence from pyroclastic couplets on Tenerife. Geol Soc Am Bull 122:305–320

Brown RJ, Bonadonna C, Durant AJ (2012) A review of volcanic ash aggregation. Phys Chem Earth 45-46:65–78

Carrasco-Núñez G, Ort MH, Romero C (2007) Evolution and hydrological conditions of a maar volcano (Atexcac crater, Eastern Mexico). J Volcanol Geotherm Res 159:179–197

Carver RE (1971) Procedures in sedimentary petrology. Wiley-Interscience, New York, p 653

Cheong CS, Choi JH, Sohn YK, Kim JC, Jeong GY (2007) Optical dating of hydromagmatic volcanoes on the southwestern coast of Jeju Island, Korea. Quat Geochron 2:266–271

Chough SK, Sohn YK (1990) Depositional mechanics and sequences of base surges, Songaksan tuff ring, Cheju Island, Korea. Sedimentology 37:1115–1135

Del Gaudio P, Mollo S, Ventura G, Iezzi G, Taddeucci J, Cavallo A (2010) Cooling rate-induced differentiation in anhydrous and hydrous basalts at 500 MPa: implications for the storage and transport of magmas in dikes. Chem Geol 270:164–178

Delpit S, Ross P-S, Jr BCH (2014) Deep-bedded ultramafic diatremes in the Missouri River breaks volcanic field, Montana, USA: 1 km of syn-eruptive subsidence. Bull Volcanol 76:832

Fisher RV (1966) Rocks composed of volcanic fragments. Earth-Sci Rev 1:287–298

Folk RL (1974) Petrology of sedimentary rocks. Hemphill Publishing Co., Austin, TX, p 182

Gernon TM, Upton BGJ, Hincks TK (2013) Eruptive history of an alkali basaltic diatreme from Elie Ness, Fife, Scotland. Bull Volcanol 75:704

Geshi N, Németh K, Oikawa T (2011) Growth of phreatomagmatic explosion craters: a model inferred from Suoana crater in Miyakejima volcano, Japan. J Volcanol Geotherm Res 201:30–38

Gilbert JS, Lane SJ (1994) The origin of accretionary lapilli. Bull Volcanol 56:398–411

Graettinger AH, Valentine GA, Sonder I, Ross P-S, White JDL, Taddeucci J (2014) Maar-diatreme geometry and deposits: subsurface blast experiments with variable explosion depth. Geochem Geophys Geosystems 15:740–764

Graettinger AH, Valentine GA, Sonder I, Ross P-S, White JDL (2015) Facies distribution of ejecta in analog tephra rings from experiments with single and multiple subsurface explosions. Bull Volcanol 77:1–12

Hahn J, Lee Y, Kim N, Hahn C, Lee S (1997) The groundwater resources and sustainable yield of Cheju volcanic island, Korea. Environ Geol 33:43–53

Heiken G, Wohletz K (1985) Volcanic ash. University of California Press, Berkeley, p 246

Helz R, Thornber C (1987) Geothermometry of Kilauea Iki lava lake, Hawaii. Bull Volcanol 49:651–668

Houghton BF, Nairn IA (1991) The 1976-1982 strombolian and phreatomagmatic eruptions of White Island, New Zealand: eruptive and depositional mechanisms at a 'wet' volcano. Bull Volcanol 54:25–49

Houghton BF, Schmincke HU (1986) Mixed deposits of strombolian and phreatomagmatic volcanism: Rothenberg volcano, East Eifel volcanic field. J Volcanol Geotherm Res 30:117–130

Houghton BF, Wilson CJN (1989) A vesicularity index for pyroclastic deposits. Bull Volcanol 51:451–462

Jeon Y, Ryu CK, Yoon W, Kang S, Song S (2013) Characteristics and interpretation of subsurface diatreme deposits from western Jeju Island. J Geol Soc Korea 49:537–551 (in Korean with English abstract)

Jeong J-O, Yoon S-H, Koh G-W, Joe Y-J, Hong J-G, Kim J-J (2016) Mineralogical and sedimentological characteristics of the U

Formation underlying the volcanic strata in Jeju Island. J Geol Soc Korea 52:389–403 (in Korean with English abstract)

Johnson ER, Wallace PJ, Cashman KV, Granados HD, Kent AJR (2008) Magmatic volatile contents and degassing-induced crystallization at Volcán Jorullo, Mexico: implications for melt evolution and the plumbing systems of monogenetic volcanoes. Earth planet. Sci Lett 269:478–487

Johnson ER, Wallace PJ, Cashman KV, Granados HD (2010) Degassing of volatiles (H_2O, CO_2, S, Cl) during ascent, crystallization, and eruption at mafic monogenetic volcanoes in Central Mexico. J Volcanol Geoth Res 197:225–238

Kim Y, Lee KS, Koh DC, Lee DH, Lee SG, Park WB, Koh GW, Woo NC (2003) Hydrogeochemical and isotopic evidence of groundwater salinization in a coastal aquifer: a case study in Jeju volcanic island, Korea. J Hydrol 270:282–294

Koh GW (1997) Characteristics of the groundwater and hydrogeologic implications of the Seoguipo formation in Cheju Island. In: Department of Geology. Pusan National University, Pusan, p 326

Koh D-C, Plummer LN, Solomon DK, Busenberg E, Kim Y-J, Chang H-W (2006) Application of environmental tracers to mixing, evolution, and nitrate contamination of ground water in Jeju Island, Korea. J Hydrol 327:258–275

Koh GW, Park JB, Kang B-R, Kim G-P, Moon DC (2013) Volcanism in Jeju Island. J Geol Soc Korea 49:209–230 (in Korean with English abstract)

Lefebvre NS, White JDL, Kjarsgaard BA (2013) Unbedded diatreme deposits reveal maar-diatreme-forming eruptive processes: standing RocksWest, Hopi Buttes, Navajo Nation, USA. Bull Volcanol 75:739

Lorenz V (1973) On the formation of maars. Bull Volcanol 37:183–204

Lorenz V (1986) On the growth of maars and diatremes and its relevance to the formation of tuff rings. Bull Volcanol 48:265–274

Luhr J (2001) Glass inclusions and melt volatile contents at Parícutin Volcano, Mexico. Contrib Mineral Petrol 142:261–283

Mair A, Hagedorn B, Tillery S, El-Kadi AI, Westenbroek S, Ha K, Koh G-W (2013) Temporal and spatial variability of groundwater recharge on Jeju Island, Korea. J Hydrol 501:213–226

Peacock MA, Fuller RE (1928) Chlorophaeite, sideromelane and palagonite from the Columbia River plateau. Am Mineral 13:360–383

Pioli L, Azzopardi BJ, Cashman KV (2009) Controls on the explosivity of scoria cone eruptions: magma segregation at conduit junctions. J Volcanol Geotherm Res 186:407–415

Poppe LJ, Eliason AH, Hastings ME (2004) A visual basic program to generate sediment grain-size statistics and to extrapolate particle distributions. Computers and Geosci 30:791–795

Pyle DM (1989) The thickness, volume and grain size of tephra fall deposits. Bull Volcanol 51:1–15

Ross P-S, White JDL (2006) Debris jets in continental phreatomagmatic volcanoes: a field study of their subterranean deposits in the Coombs Hills vent complex, Antarctica. J Volcanol Geotherm Res 149:62–84

Ross PS, White JDL, Zimanowski B, Buettner R (2008) Multiphase flow above explosion sites in debris-filled volcanic vents: insights from analogue experiments. J Volcanol Geotherm Res 178:104–112

Ross P-S, Delpit S, Haller MJ, Németh K, Corbella H (2011) Influence of the substrate on maar–diatreme volcanoes — an example of a mixed setting from the Pali Aike volcanic field, Argentina. J Volcanol Geotherm Res 201:253–271

Ross P-S, White JDL, Valentine GA, Taddeucci J, Sonder I, Andrews RG (2013) Experimental birth of a maar-diatreme volcano. J Volcanol Geotherm Res 260:1–12

Rosseel J-B, White JDL, Houghton BF (2006) Complex bombs of phreatomagmatic eruptions: Role of agglomeration and welding in vents of the 1886 Rotomahana eruption, Tarawera, New Zealand. J Geophys Res 111(B12205):doi:10.1029/2005JB004073

Sable JE, Houghton BF, Del Carlo P, Coltelli M (2006) Changing conditions of magma ascent and fragmentation during the Etna 122 BC basaltic Plinian eruption: evidence from clast microtextures. J Volcanol Geoth Res 158:333–354

Schumacher R, Schmincke HU (1995) Models for the origin of accretionary lapilli. Bull Volcanol 56:626–639

Shinn YJ, Chough SK, Kim JW, Woo J (2007) Development of depositional systems in the southeastern Yellow Sea during the postglacial transgression. Mar Geol 239:59–82

Sohn YK (1996) Hydrovolcanic processes forming basaltic tuff rings and cones on Cheju Island, Korea. Geol Soc Am Bull 108:1199–1211

Sohn YK (2015) A study of the plan to reduce erosion of natural monuments in the coastal areas of Jeju Island. National Research Institute of Cultural Heritage, Daejeon, p 286

Sohn YK, Park KH (2004) Early-stage volcanism and sedimentation of jeju island revealed by the Sagye Borehole, SW Jeju Island, Korea. Geosci J 8:73–84

Sohn YK, Park KH (2005) Composite tuff ring/cone complexes in Jeju Island, Korea: possible consequences of substrate collapse and vent migration. J Volcanol Geotherm Res 141:157–175

Sohn C, Sohn YK (2016) Sedimentary record of a 4 ka B.P. storm event preserved within the rimbeds of a coastal tuff ring in Jeju Island, Korea. In: The 6th International Maar Conference. Changchun, China

Sohn YK, Park JB, Khim BK, Park KH, Koh GW (2002) Stratigraphy, petrochemistry and Quaternary depositional record of the Songaksan tuff ring, Jeju Island, Korea. J Volcanol Geotherm Res 119:1–20

Sohn YK, Park KH, Yoon SH (2008) Primary versus secondary and subaerial versus submarine hydrovolcanic deposits in the subsurface of Jeju Island, Korea. Sedimentology 55:899–924

Sohn YK, Cronin SJ, Brenna M, Smith IEM, Nemeth K, White JDL, Murtagh RM, Jeon YM, Kwon CW (2012) Ilchulbong tuff cone, Jeju Island, Korea, revisited: a compound monogenetic volcano involving multiple magma pulses, shifting vents, and discrete eruptive phases. Geol Soc Am Bull 124:259–274

Sohn YK, Yoon WS, Ahn US, Kim GB, Lee J-H, Ryu CK, Jeon YM, Kang CH (2015) Stratigraphy and age of the human footprints-bearing strata in Jeju Island, Korea: controversies and new findings. J Archaeol Sci Rpt 4:264–275

Son M, Kim JS, Jung S, Ki JS, Kim MC, Sohn YK (2012) Tectonically controlled vent migration during maar-diatreme formation: an example from a Miocene half-graben basin in SE Korea. J Volcanol Geotherm Res 223:29–46

Sottili G, Taddeucci J, Palladino DM, Gaeta M, Scarlato P, Ventura G (2009) Sub-surface dynamics and eruptive styles of maars in the Colli Albani Volcanic District, Central Italy. J Volcanol Geotherm Res 180:189–202

Sparks RSJ, Walker GPL (1977) The significance of vitric-enriched air-fall ashes associated with crystal-enriched ignimbrites. J Volcanol Geotherm Res 2:329–341

Taddeucci J, Pompilio M, Scarlato P (2004) Conduit processes during the July-August 2001 explosive activity of Mt. Etna (Italy): inferences from glass chemistry and crystal size distribution of ash particles. J Volcanol Geotherm Res 137:33–54

Taddeucci J, Sottili G, Palladino DM, Ventura G, Scarlato P (2010) A note on maar eruption energetics: current models and their application. Bull Volcanol 72:75–83

Taddeucci J, Valentine GA, Sonder I, White JDL, Ross P-S, Scarlato P (2013) The effect of pre-existing craters on the initial development of explosive volcanic eruptions: an experimental investigation. Geophys Res Lett 40:507–510

Valentine GA (2012) Shallow plumbing systems for small-volume basaltic volcanoes, 2: evidence from crustal xenoliths at scoria cones and maars. J Volcanol Geotherm Res 223-224:47–63

Valentine GA, White JDL (2012) Revised conceptual model for maar-diatremes: subsurface processes, energetics, and eruptive products. Geology 40:1111–1114

Valentine GA, Graettinger AH, Sonder I (2014) Explosion depths for phreatomagmatic eruptions. Geophys Res Lett 41:3045–3051

Valentine GA, Graettinger AH, Macorps E, Ross P-S, White JDL, Döhring E, Sonder I (2015) Experiments with vertically and laterally migrating subsurface explosions with applications to the geology of phreatomagmatic and hydrothermal explosion craters and diatremes. Bull Volcanol 77:1–17

Vespermann D, Schmincke H-U (2000) Scoria cones and tuff rings. In: Sigurdsson H, Houghton BF, McNutt SR, Rymer H, Stix J (eds) Encyclopedia of Volcanoes. Academic Press, San Diego, pp 683–694

Walker GPL (1972) Crystal concentration in ignimbrites. Contri Mineral Petrol 36:135–146

White JDL (1991) Maar-diatreme phreatomagmatism at Hopi Buttes, Navajo Nation (Arizona), USA. Bull Volcanol 53:239–258

White JDL (1996) Impure coolants and interaction dynamics of phreatomagmatic eruptions. J Volcanol Geotherm Res 74: 155–170

White JDL, Houghton B (2000) Surtseyan and related phreatomagmatic eruptions. In: Sigurdsson H, Houghton BF, McNutt SR, Rymer H, Stix J (eds) Encyclopedia of Volcanoes. Academic Press, San Diego, pp 495–511

White JDL, Houghton BF (2006) Primary volcaniclastic rocks. Geology 34:677–680

White JDL, Ross P-S (2011) Maar-diatreme volcanoes: a review. J Volcanol Geotherm Res 201:1–29

Won J-H, Kim J-W, Koh G-W, Lee J-Y (2005) Evaluation of hydrogeological characteristics in Jeju Island, Korea. Geosci J 9:33–46

Won J-H, Lee J-Y, Kim J-W, Koh G-W (2006) Groundwater occurrence on Jeju Island, Korea. Hydrogeol J 14:532–547

Yoon WS, Yoon SH, Sohn C, Sohn YK (2016) Records of palaeo-sea level and eruption duration in a coastal tuff ring in Jeju Island, Korea. Terra Nova:accepted (DOI: 10.1111/ter.12248)

Zimanowski B, Buttner R (2002) Dynamic mingling of magma and liquefied sediments. J Volcanol Geoth Res 114:37–44

Zimanowski B, Buttner R, Lorenz V (1997) Premixing of magma and water in MFCI experiments. Bull Volcanol 58:491–495